Physica D 298–299 (2015) 48–67

Contents lists available at ScienceDirect

Physica D

journal homepage: www.elsevier.com/locate/physd

Tracking pattern evolution through extended center manifold reduction and singular perturbations

L. Sewalt [a,*], A. Doelman [a], H.G.E. Meijer [b], V. Rottschäfer [a], A. Zagaris [b]

[a] Leiden University, Niels Bohrweg 1, 2333 CA Leiden, The Netherlands
[b] University of Twente, P.O. Box 217, 7500 AE Enschede, The Netherlands

ARTICLE INFO

Article history:
Received 16 April 2014
Received in revised form
25 October 2014
Accepted 25 January 2015
Available online 7 February 2015
Communicated by Y. Nishiura

Keywords:
Pattern formation
Low-dimensional chaos
Dimension reduction

ABSTRACT

In this paper we develop an extended center manifold reduction method: a methodology to analyze the formation and bifurcations of small-amplitude patterns in certain classes of multi-component, singularly perturbed systems of partial differential equations. We specifically consider systems with a spatially homogeneous state whose stability spectrum partitions into eigenvalue groups with distinct asymptotic properties. One group of successive eigenvalues in the bifurcating group are widely interspaced, while the eigenvalues in the other are stable and cluster asymptotically close to the origin along the stable semi-axis. The classical center manifold reduction provides a rigorous framework to analyze destabilizations of the trivial state, as long as there is a spectral gap of sufficient width. When the bifurcating eigenvalue becomes commensurate to the stable eigenvalues clustering close to the origin, the center manifold reduction breaks down. Moreover, it cannot capture subsequent bifurcations of the bifurcating pattern. Through our methodology, we formally derive expressions for low-dimensional manifolds exponentially attracting the full flow for parameter combinations that go beyond those allowed for the (classical) center manifold reduction, i.e. to cases in which the spectral gap condition no longer can be satisfied. Our method also provides an explicit description of the flow on these manifolds and thus provides an analytical tool to study subsequent bifurcations. Our analysis centers around primary bifurcations of transcritical type – that can be either of co-dimension 1 or 2 – in two- and three-component PDE systems. We employ our method to study bifurcation scenarios of small-amplitude patterns and the possible appearance of low-dimensional spatio-temporal chaos. We also exemplify our analysis by a number of characteristic reaction–diffusion systems with disparate diffusivities.

1. Introduction

The analysis of pattern formation in evolutionary partial differential equations is directly linked to dynamical systems bifurcation theory. At the onset of patterns, a '*trivial state*' becomes spectrally unstable as a control or bifurcation parameter, R, passes through a critical value $R_{c,1}$. Typically, a '*small amplitude pattern*' bifurcates from this state. When the evolution equation is defined on a bounded domain Ω and the associated spectrum consists of discrete eigenvalues, the very first step in the onset of pattern formation can be studied by a center manifold reduction (CMR). For values of R sufficiently close to $R_{c,1}$, the dynamics of the full infinite-dimensional system can be reduced to the dynamics on an exponentially attracting low-dimensional center manifold, by virtue of the existence of a spectral gap between the first eigenvalue(s) crossing the imaginary axis and all other, stable eigenvalues. The presence of this gap makes the analysis of the onset of pattern formation completely equivalent to the study of bifurcations in finite-dimensional dynamical systems (for instance, [1–3]). Indeed, the small amplitude patterns that originate in this mechanism relate, in general, directly to the standard codimension 1 bifurcations (saddle–node, transcritical, pitchfork and Hopf): the associated center manifolds are 1- or 2-dimensional.

The center manifold reduction is only valid for R '*sufficiently close*' to the – first – critical value $R_{c,1}$, so that the spectral gap is sufficiently wide. However, in perhaps all examples of pattern forming systems, the pattern originating at $R_{c,1}$ undergoes a next bifurcation at some value $R_{c,2}$ of R et cetera. In other words, the first bifurcation at onset is followed by a secondary one at $R_{c,2}$. Since this latter concerns the bifurcating pattern and not the trivial state it bifurcated from, it cannot be directly studied through the

* Corresponding author.
E-mail address: lotte@math.leidenuniv.nl (L. Sewalt).

http://dx.doi.org/10.1016/j.physd.2015.01.006
0167-2789/

spectral decomposition for that state. One now needs, instead, stability properties of the pattern bifurcating at $R_{c,1}$. Generally speaking, this is an impossible task — especially for analytical studies of pattern evolution. To overcome that obstacle, formal and/or numerical methods have been developed that are based on spectral properties – eigenvalues and eigenfunctions – associated with the original, trivial background state.

Such secondary, tertiary, et cetera subsequent bifurcations cannot be described by CMR, simply because they do not occur in the reduced (center manifold) flow. Therefore, they take place for values of R violating the spectral gap condition. This is often observed in an explicit setting: the distance between the first, now unstable, eigenvalue and the imaginary axis becomes proportional to that between the next largest eigenvalue(s) and the same axis — note carefully that none of these next eigenvalues needs to destabilize for the secondary bifurcation to occur. In the terminology of applied mathematics and/or physics: one *must* account for the evolution of '*modes*' associated with these next eigenvalues and eigenfunctions, as these modes can no longer be '*slaved*' to the one that was first destabilized and that parameterizes the center manifold. In principle, then, studying the full flow through the spectral properties of the trivial state is possible, provided that one extends CMR to a higher-dimensional system by a Galerkin approach. In general, however, there is no '*next*' spectral gap in that extended spectral problem: *all* next eigenvalues are typically commensurable. Accordingly, there is no telling a priori *how many* modes must be accounted for in this extended center manifold Galerkin reduction — certainly not from the analytic point of view. See, for instance, [4] and references therein for a practical study centering on these issues.

Presently, we develop analytical (and asymptotic) extensions of classical CMR. We describe the onset of pattern formation by means of low-dimensional systems governing the dynamics of the full evolutionary system for parameter values violating the spectral gap condition. We term the process by which we derive such simplified systems *extended center manifold reduction (ECMR)*. Our most generic results concern the extension of the 1-dimensional CMR associated with a transcritical bifurcation to an explicit 2-dimensional flow on an exponentially attracting 2-dimensional (local) manifold. We also present explicit classes of systems with codimension 1 bifurcations where this extended center manifold is 3- or 4-dimensional.

An earlier version of this method was developed in the context of a specific model problem, which concerned the emergence and evolution of localized spatio-temporal patterns in a non-local, coupled, phytoplankton-nutrient model in an oceanic setting,

$$\begin{cases} \omega_t = \varepsilon\omega_{xx} - 2\sqrt{\varepsilon}v\omega_x + (p(\omega,\eta,x) - \ell)\omega, \\ \eta_t = \varepsilon\left[\eta_{xx} + \ell^{-1}p(\omega,\eta,x)\omega\right]; \end{cases} \tag{1.1}$$

this is a scaled version of the original model proposed in [5]. In (1.1), $\omega(x,t)$ and $\eta(x,t)$ denote a phytoplankton and a (translated) nutrient concentration; $x \in (0,1)$ measures ocean depth. The growth of the phytoplankton population is delimited by nutrient and light availability; since light is attenuated with depth and absorbed by phytoplankton, the term $p(\omega,\eta,x)$ is non-local in ω and depends explicitly on depth x. For more details on this model and its boundary conditions (BCs), see [5–7]. In realistic settings, $\varepsilon \approx 10^{-5}$ while all other parameters — v, ℓ and those entering $p(\omega,\eta,x)$ — can be considered $\mathcal{O}(1)$ with respect to ε [6]. Therefore, (1.1) is studied in [6,7] as a *singularly perturbed* system. The spectral problem associated with the stability of the trivial state $(\omega(x,t),\eta(x,t)) \equiv (0,0)$ — no phytoplankton, maximal and constant nutrient concentration — has two distinct sets of (real) eigenvalues: $\mu_m = \mathcal{O}(\varepsilon)$, $m \geq 1$, and $\lambda_n = \lambda_* + \tilde{\lambda}_n$, with $\tilde{\lambda}_n = \mathcal{O}(\varepsilon^{\frac{1}{3}})$ and $n \geq 1$; λ_* can be '*controlled*' by varying the parameters in (1.1), while $\mu_m < 0$ are parameter-independent and negative. In [6], it is shown through an asymptotic spectral analysis that the trivial state is destabilized by a transcritical bifurcation, at which λ_1 crosses zero. The associated eigenfunction has the strongly localized nature of a (stationary) *deep chlorophyll maximum* (DCM), the pattern playing a central role in the simulations and oceanic observations in [5].

In our terminology above, emergence of the deep chlorophyll maximum represents the onset of pattern formation, and it occurs as the product of the first bifurcation. For the parameter values considered in [5], the deep chlorophyll maximum only exists (as a stable, stationary pattern) in an asymptotically narrow strip of parameter space: the primary bifurcation is almost directly followed by a secondary, Hopf bifurcation through which emerges an oscillating deep chlorophyll maximum [6,7]. In fact, stationary deep chlorophyll maxima were not even recorded in the numerical simulations of [5] — the bifurcation scenario drawn there starts directly with the oscillating deep chlorophyll maximum and proceeds with period-doubling cascades and spatio-temporal chaos. In other parameter regimes, not a deep chlorophyll maximum, but a *benthic layer* — a localized maximum at ocean's bottom — marks pattern formation. Numerical simulations have not indicated a secondary bifurcation of the pattern in this regime. In [8], we analytically substantiate this phenomenon using the framework described in this treatise.

The predictions in [6] on the transcritical nature of trivial state destabilization were validated in [7], as a first step, by restricting analysis to the regime $0 < \lambda_1 = \mathcal{O}(\varepsilon^\sigma)$ with $\sigma > 1$. In that case, there is a spectral gap driven by the proximity of that primary eigenvalue to the imaginary axis, $\lambda_1 \ll \min_{m\geq 1, n\geq 2}\{|\mu_m|, |\lambda_n|\} = \mathcal{O}(\varepsilon)$; the dynamics of system (1.1) can be reduced to a single amplitude ODE describing the transcritical bifurcation. As $\sigma \downarrow 1$ and λ_1 becomes $\mathcal{O}(\varepsilon)$ like the μ_m's, the spectral gap dissolves; modes associated with *all* (linearly stable!) μ_m-eigenvalues must now be taken into account. As a consequence, the 1-dimensional CMR is expanded dramatically into an a priori infinite-dimensional system. Analysis of that model is nevertheless possible and establishes the existence of a secondary Hopf bifurcation in (1.1), $\mathcal{O}(\varepsilon)$-close to the primary, transcritical one [7]. The existence of oscillating deep chlorophyll maxima follows.

In the present paper, we show that this surprising fact — that a secondary bifurcation becomes amenable to analysis by extending CMR beyond its classical region of validity — is not due to model specifics but intrinsically tied to the nature of the spectrum associated with the trivial background state. In general, our approach may be developed in the context of systems of the form

$$\frac{\partial}{\partial t}\begin{pmatrix} U \\ V \end{pmatrix} = \begin{pmatrix} \mathcal{L} & 0 \\ \varepsilon\mathcal{K} & \varepsilon\mathcal{M} \end{pmatrix}\begin{pmatrix} U \\ V \end{pmatrix} + \begin{pmatrix} F(U,V;x) \\ \varepsilon G(U,V;x) \end{pmatrix}, \tag{1.2}$$

for a 'fast', unknown $U : \Omega \times \mathbb{R}_+ \to \mathbb{R}^{m_U}$ and a 'slow' $V : \Omega \times \mathbb{R}_+ \to \mathbb{R}^{m_V}$, with $m_U, m_V \geq 1$. The bounded spatial domain $\Omega \subset \mathbb{R}^n$ has a piecewise C^1 boundary $\partial\Omega$. The operators $\mathcal{K}$, $\mathcal{L}$ and $\mathcal{M}$ are assumed linear, spatial, differential operators and boundary conditions guaranteeing well-posedness must apply. Several specific assumptions on the spectrum of $\mathcal{L}$ and $\mathcal{M}$ and the nonlinearities $F(U,V;x)$ and $G(U,V;x)$ must hold, we refer to [8] for more details. The aim of this paper is to present an exploration into the possible impact of the extended center manifold reduction approach. Therefore, we will mainly restrict our analysis to a strongly simplified version of (1.2), i.e. to models of the type

$$\begin{cases} U_t = \mathcal{L}U + \alpha U + F(U,V), \\ V_t = \varepsilon\left[\mathcal{L}V + \beta U + \gamma V + G(U,V)\right], \end{cases} \tag{1.3}$$

thus $\mathcal{K} = \beta$, and with a slight abuse of notation, $\mathcal{M} = \mathcal{L} + \gamma$ and the operator $\mathcal{L}$ in (1.2) will be replaced by $\mathcal{L} + \alpha$. The linear differential operator $\mathcal{L}$ in (1.3) — independent of ε — acts on $L^2(\Omega)$,

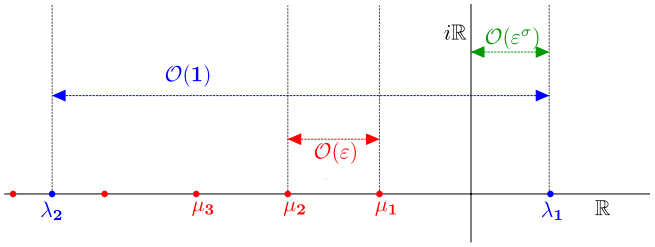

Fig. 1.1. Schematic representation of the eigenvalues that determine the stability of $(U, V) = (0, 0)$. The eigenvalues divide into two separate sets. One set of infinitely many $\mathcal{O}(1)$-interspaced eigenvalues, λ_k, and one set of infinitely many $\mathcal{O}(\varepsilon)$-interspaced eigenvalues, μ_k. Here, the parameter values are such that all μ_k are negative, while the first $\mathcal{O}(1)$ eigenvalue crossed into the right half-plane but remains small, $\mathcal{O}(\varepsilon^\sigma)$ with $\sigma > 0$.

contains spatial derivatives only and is assumed self-adjoint with respect to given boundary conditions. We mostly restrict ourselves to the scalar case $m_U = m_V = 1$. In Section 6, however, we will treat an example where $m_U = 2$. By assuming that $0 < \varepsilon \ll 1$ is asymptotically small, system (1.3) becomes singularly perturbed; the parameters $\alpha, \beta, \gamma \in \mathbb{R}$ are assumed $\mathcal{O}(1)$ with respect to ε. The functions $F(U, V)$ and $G(U, V)$ are assumed sufficiently smooth and at least quadratic in U and V. The Laplace operator Δ subject to Dirichlet boundary conditions is a natural choice for $\mathcal{L}$, with (1.3) then becoming a reaction–diffusion system. This choice is considered in Sections 2.2, 4.2, 5.2 and 6.2 to add concreteness to our discussion, but it is not the sole focus of the present work: precise assumptions on $\mathcal{L}$ and Ω are given in Section 2.

One may see the simplified model (1.3) as stripping the explicit phytoplankton model (1.1) of its non-locality, heterogeneity and various other intricacies not central to our stated aim. It is for that reason that (1.1) does not precisely fit the framework (1.3). However, it does fit (1.2), and we elaborate further on this in [8]. The main property carried over from (1.1) to (1.3), and also crucial to (1.2), is a decomposition of the (real) eigenvalues in the spectral problem determining stability of the trivial state $(U, V) \equiv (0, 0)$ into distinct, ordered, '*small*' and '*large*' sets

$$\mu_k = \mathcal{O}(\varepsilon), \quad \text{and} \quad \lambda_k = \mathcal{O}(1), \quad k \geq 1; \tag{1.4}$$

cf. Section 2 and Fig. 1.1. It should be noted here that, strictly speaking, only asymptotically many μ_k's and λ_k's are $\mathcal{O}(\varepsilon)$, as both sequences diverge to $-\infty$. Similarly to [7], we focus on the destabilization of $(0, 0)$ by the '*most unstable*' large eigenvalue λ_1, assuming that all other eigenvalues remain in the left half of the complex plane. As in (1.1), destabilization of $(0, 0)$ at $\lambda_1 = 0$ in general occurs through a transcritical bifurcation. This is evident through a standard center manifold reduction, yet we consciously employ a slightly different, equivalent approach as a means of setting the stage for Sections 4.1 and 4.2; see Section 3.2 for details.

For our abstract model (cf. Fig. 1.1), center manifold reduction remains valid while $\sigma > 1$ just as for (1.1); it breaks down at $\sigma = 1$, recall our discussion above on the commensurability of λ_1 and $\mu_1, \mu_2, \ldots$, where we also briefly mentioned an extension of the 1-dimensional center manifold reduction to an infinite-dimensional Fourier system. A Fourier decomposition links every eigenvalue λ_i and μ_i to a corresponding eigenfunction with amplitudes $a_i(t)$ and $b_i(t)$, respectively. Concretely, this means that the ODE governing the evolution in (scaled) time τ of the (scaled) amplitude $a_1(\tau)$ of the λ_1-eigenmode must, now, be combined with ODEs for $b_k(\tau), k \geq 1$ — the (scaled) amplitudes of the μ_k-eigenmodes. One of the main results in this paper is the identification at leading order in ε of a 2-dimensional, exponentially attracting, invariant submanifold for this infinite-dimensional system. Thus, also for $\sigma = 1$, the dynamics of small, $\mathcal{O}(\varepsilon)$ solutions of (1.3) is contained in a low-dimensional manifold. However, in contrast to the region of classical CMR validity, the dimension of that manifold is 2. As we will see, this increase in the dimensionality of the reduced flow lies at the heart of complex phenomena exhibited by the dynamics of small amplitude solutions of (1.3).

The invariant manifold is parameterized by the modes (a_1, b_1) and the flow on it is explicitly deducible. A straightforward analysis reveals that the original pattern bifurcating at onset generically undergoes a Hopf bifurcation, provided that equation coefficients satisfy an explicit sign condition. It follows that the primary transcritical bifurcation is generically followed within an $\mathcal{O}(\varepsilon)$ distance by a Hopf bifurcation, exactly as in the phytoplankton model. The sub-/supercritical nature of this bifurcation can also be determined. We finally show that, in such an event, the bifurcating oscillatory pattern necessarily terminates as the control parameter moves further away from both bifurcations (transcritical and Hopf), leaving the attracting 2-dimensional manifold unable to sustain bounded behavior. Note that this entire sequence plays out ε-close to the primary bifurcation in parameter space. In that manner, our analysis provides an explicit bound on the region in parameter space where small-amplitude center manifold may be extended: outside it, solutions to the full problem (1.3) can no longer remain small. This is in stark contrast to standard CMR, which cannot provide such an explicit bound.

In the phytoplankton-nutrient model (1.1), the first two bifurcations are only the first steps in a sequence of events leading to low-dimensional spatio-temporal chaos [5]. We investigate the possibility of similar behavior in singularly perturbed systems (1.3) in the second half of the present paper. Our results so far indicate that, near the primary bifurcation, small pattern dynamics are inherently 2-dimensional and hence cannot exhibit such phenomena. Even worse, Hopf destabilization of the primary pattern — the second step in the chaotic scenario of (1.1) — is followed by unbounded dynamics: if more complex dynamics is present, it does not play out on the extended center manifold. In contrast, the dimensionality of the long-term dynamics in (1.1) is less clear-cut, and the Hopf destabilization was deduced from a high-dimensional reduced system. Additionally, it was speculated in [7] already that a codimension 2 transcritical bifurcation in (1.1) may be the organizing center of its spatio-temporal chaotic dynamics. Inspired by these observations, we move on from the most simple case of (1.3) and consider two types of systems: first, one with amplified nonlinearities; and second, one where the primary bifurcation is of codimension 2; see Sections 5 and 6 for further motivation.

To motivate the first direction, we ascertain that it is the *linear* structure of (1.3) that enables our approach — not the particular form of the nonlinearities. Hence, the introduction of an $\mathcal{O}(1)$ nonlinearity in the PDE for V should not hinder application of our method, and we consider (1.3) with an $\mathcal{O}(1)$ nonlinearity $G(U, V)$ replacing $\varepsilon G(U, V)$; see especially system (5.1). This leaves the linear structure unaltered but affects the dimensionality of the reduction strongly. The extended invariant manifold is no longer 2-dimensional; in fact, asymptotically many b_k-modes — related to the 'small' spectrum $\{\mu_k\}_{k\geq 1}$ — are excited and must be included in the reduced system, resembling the situation in (1.1). As an exploratory example, we consider $G(U, V) = G_{20}U^2$ and '*tune*' G_{20} by having it depend on x, see Section 5.2. In that way, we construct (at leading order in ε) an attracting, linear, 5-dimensional, extended center manifold and describe the flow on it by means of the quintuplet $(a_1, b_1, b_2, b_3, b_4)$. Here a_1 and b_i, $i = 1 \ldots 4$ are the (rescaled) amplitudes associated with λ_1 and μ_i, respectively. The most unstable mode — which, local to onset, is spanned by a_1 — successfully undergoes a Hopf bifurcation. Depending on parameter values, this Hopf bifurcation can be followed by a sequence of period-doublings resulting in chaotic behavior; recall that this is exactly the case in (1.1). This last result is established numerically, with direct PDE simulations within the chaotic regime revealing a low-dimensional spatio-temporal attractor strikingly similar to

the one capturing trajectories of the 5-dimensional reduced flow; see Fig. 5.3. We conclude that the ECMR accurately describes the dynamics of small amplitude solutions to (5.1), even when this is complex.

Regarding the second direction, we note that the codimension 2 transcritical bifurcation in (1.1) arises as the merging of two transcritical bifurcations generating different localized patterns — a deep chlorophyll maximum (DCM) and a *benthic layer* (BL). We emulate this situation here by tuning the two-component model (1.3) so that the two largest $\mathcal{O}(1)$ eigenvalues, λ_1 and λ_2, coincide at the origin and the corresponding eigenfunctions are distinct — i.e., the system is *not* in the most general case where one needs to introduce a generalized eigenfunction. Extending the standard center manifold to the '*gapless*' situation in which $\lambda_1, \lambda_2, \mu_k = \mathcal{O}(\varepsilon)$, we obtain a leading order, attracting, 4-dimensional, extended center manifold parameterized by (a_1, a_2, b_1, b_2) — the rescaled amplitudes of modes related to $\lambda_1, \lambda_2, \mu_1$ and μ_2, respectively — and the flow on that extended center manifold. See also (6.7) and its rich behavior we analyze in Section 6. Note, however, that $\mathcal{L} = \Delta$ does not admit a double zero eigenvalue, but examples of (polyharmonic) operators satisfying both conditions are available; see [9] for these facts. Since our prior discussion is rooted in reaction–diffusion systems, we consider in parallel a three-component, reaction–diffusion system of the form (1.3) that admits a double zero eigenvalue. We keep our model as simple as possible, creating a codimension 2 bifurcation by introducing a *vectorial* '*fast*' component U,

$$\begin{cases} \partial_t U_1 = D_1 \mathcal{L} U_1 + \alpha_1 U_1 + F_1(U_1, U_2, V), \\ \partial_t U_2 = D_2 \mathcal{L} U_2 + \alpha_2 U_2 + \varepsilon \rho_2 V + F_2(U_1, U_2, V), \\ \partial_t V = \varepsilon \left[\mathcal{L} V + \beta_1 U_1 + \beta_2 U_2 + \gamma V + G(U_1, U_2, V) \right]; \end{cases} \tag{1.5}$$

see Section 6.2 for more details on this model and its boundary conditions. There exist two sets of large, $\mathcal{O}(1)$ eigenvalues, $\lambda_{1,k}$ and $\lambda_{2,k}$ ($k \geq 1$), where $\lambda_{1,k}$ relates to the linear spectrum of the first equation of (1.5), and $\lambda_{2,k}$ relates to the linear spectrum of the second equation of (1.5). The codimension 2 bifurcation corresponds to the regime $\lambda_{1,1} \approx \lambda_{2,1} \approx 0$. Extending the center manifold, to encompass the regime where $\lambda_{1,1}, \lambda_{2,1}$ and asymptotically many μ_k's are $\mathcal{O}(\varepsilon)$ yields an attracting 3-dimensional manifold parameterized by $(a_{1,1}, a_{2,1}, b_1)$. The (rescaled) amplitudes $a_{1,1}(t)$, $a_{2,1}(t)$ and $b_1(t)$ are associated with the eigenvalues $\lambda_{1,1}, \lambda_{2,1}$ and μ_1, respectively and denote the amplification in the corresponding modes of a Fourier-like decomposition, see (6.10). The flow on it is generated by a rather general quadratic vector field – see (6.21) – containing the celebrated Lorenz system [10] as a special case. A simulation of the full PDE system (1.5) motivated by the classical parameter settings in [10] directly captures the Lorenz attractor; see Fig. 1.2. We stress, however, an essential difference between the role of the Lorenz equations relative to the global dynamics here and in [10]. According to our theory, the Lorenz attractor is a global attractor for the (small amplitude) flow induced by the full model (1.5); numerical simulations confirm this, see Fig. 1.2. Instead, the same attractor does not attract trajectories of the corresponding convection model in [10], although the Lorenz equations are derived from it through a Galerkin-type reduction — [11], for instance, discusses the differentiating influence of higher-order Galerkin modes. Small amplitude derivations of the Lorenz system (e.g., [12]) only concern solutions with special characteristics, and thus they also do not result in a 3-dimensional flow approximating the full, infinite-dimensional one.

As already mentioned at various places in this Introduction, the analysis presented in this paper is exploratory and formal. Theorems and propositions are provided with proofs, while claims and conjectures are not. We conclude the paper with a brief discussion of future plans, including rooting this analysis on a rigorous foundation, and of the relevance of our study for phenomena reported in the (mostly reaction–diffusion oriented) literature.

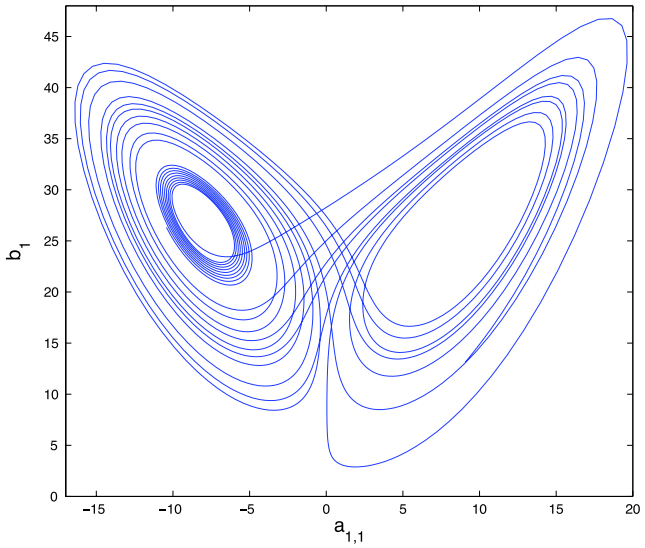

Fig. 1.2. Simulation of system (1.5) using MATLAB's PDEPE function with $\mathcal{L} = \Delta$, $\Omega = (0, 1)$ and Dirichlet BCs. Here, $\varepsilon = 0.01$, $D_1 = D_2 = 1$, $\alpha_1 = \pi^2 - 8\varepsilon/3$, $\alpha_2 = \pi^2 - \varepsilon$, $\beta_1 = 0$, $\beta_2 = 10$, $\gamma = \pi^2 - 10$ and $\rho_2 = 28$. The nonlinearities are $F_1(U, V) = (3\sqrt{2}\pi/16)U_2 V$, $F_2(U, V) = -(3\sqrt{2}\pi/16)U_1 V$ and $G(U, V) = U_1^2$. Plotted are the rescaled amplitudes $a_{1,1}(t)$ and $b_1(t)$, (see (6.10)), of the full solution $(U_1(x, t), U_2(x, t), V(x, t))$ of system (1.5).

2. Spectral analysis of the trivial state

The key to analyzing (1.3) is explicit control over the spectrum and associated eigenfunctions of the linearization around the background state $(U, V) = (0, 0)$. In this section, we formulate the properties that this spectrum must have to enable our analysis; these effectively formalize Fig. 1.1. Then, to illustrate these properties, we introduce a reaction–diffusion example in Section 2.2, working out its spectrum methodically.

2.1. Linear stability

We write the PDE system (1.3) in matrix form, separating the linear and nonlinear parts,

$$\begin{aligned} \begin{pmatrix} U \\ V \end{pmatrix}_t &= \begin{pmatrix} \mathcal{L} + \alpha & 0 \\ \varepsilon\beta & \varepsilon(\mathcal{L} + \gamma) \end{pmatrix} \begin{pmatrix} U \\ V \end{pmatrix} + \begin{pmatrix} F(U, V) \\ \varepsilon G(U, V) \end{pmatrix} \\ &= \mathcal{D}\mathcal{T} \begin{pmatrix} U \\ V \end{pmatrix} + \mathcal{N}(U, V). \end{aligned} \tag{2.1}$$

The linear stability of solution $(0, 0)$ is governed by the spectral problem associated with $\mathcal{D}\mathcal{T}$,

$$\Lambda u = \mathcal{L} u + \alpha u, \tag{2.2a}$$

$$\Lambda v = \varepsilon \mathcal{L} v + \varepsilon\beta u + \varepsilon\gamma v. \tag{2.2b}$$

Next, we impose boundary conditions and formulate necessary conditions on the operator $\mathcal{L} : H \to H$ acting on an appropriate Hilbert space H equipped with the standard L^2-inner product. Consider the scalar spectral problem of $\mathcal{L}$,

$$\mathcal{L}\phi(x) = \nu\phi(x), \tag{2.3}$$

where ν is an eigenvalue and $\phi \in H$ is a scalar eigenfunction, i.e. $\phi(x) \in \mathbb{R}$, satisfying boundary conditions adapted from (2.1). We recall that $\mathcal{L}$ does not depend on ε and assume:

A1 $\mathcal{L}$ is self-adjoint.

A2 The solutions of (2.3) (eigenvalues of $\mathcal{L}$) are ordered with a maximal element,

$$\cdots \leq \nu_3 \leq \nu_2 \leq \nu_1 < \infty.$$

A3 The invariant subspace associated with any eigenvalue ν_k is one-dimensional.

Moreover, we assume that the boundary conditions are the same for U and V on $\partial\Omega$.

In Section 2.2, we will introduce an explicit example system with $\mathcal{L} = \Delta$ and $H = H_0^1(0,1)$, the Sobolev space of compactly supported, weakly differentiable functions. Assumptions A1–A2 are automatically satisfied in this case — see [13]. Note that A3, on the other hand, is somewhat strong, as it entails that we do not need to introduce generalized eigenvectors in the case of repeated eigenvalues. In Section 6, we will see specific examples by setting $\mathcal{L} = -\Delta^2$ and $H = H_0^2(A_\delta)$ on an annulus $A_\delta = \left\{(x,y) \in \mathbb{R}^2 : \delta^2 < x^2 + y^2 < 1\right\}$, $0 < \delta < 1$. The boundary condition is $U = V = 0$ and $\nabla U = \nabla V = 0$ on $\partial\Omega$ [9]. In Remark 4.2, we will comment briefly on more general systems that do not satisfy the assumptions above but are nevertheless expected to generate dynamics beyond the classical CMR similar to model (1.3) — such as the phytoplankton-nutrient model (1.1).

The solutions of equations (2.2) and associated BCs are eigenvectors $(u(x), v(x))^T$ and associated eigenvalues Λ. These eigenvalues are all real-valued, due to the triangular structure of $\mathcal{DT}$ and the condition that $\mathcal{L}$ is self-adjoint. As a matter of fact, solutions to the full spectral problem (2.2) are expressible in terms of the solutions to (2.3).

We normalize the eigenfunctions under the norm of $L^2(\Omega)$,

$$\langle \phi_k, \phi_l \rangle_{L^2} = \delta_{kl}, \quad \text{with } \delta_{kl} \text{ the Kronecker delta.}$$

We define the function space $\mathcal{H}$ spanned by the eigenfunctions of $\mathcal{L}$,

$$\mathcal{H} = \mathrm{cl}\left\{ \mathrm{span}\left\{\{\phi_k\}_{k\geq 1}\right\} \times \mathrm{span}\left\{\{\phi_k\}_{k\geq 1}\right\} \right\}, \tag{2.4}$$

define on it an inner product for a Cartesian product of L^2-spaces,

$$\left\langle \begin{pmatrix} u_1(x) \\ v_1(x) \end{pmatrix}, \begin{pmatrix} u_2(x) \\ v_2(x) \end{pmatrix} \right\rangle_{\mathcal{H}} = \int_\Omega \left(u_1(x)u_2(x) + v_1(x)v_2(x)\right)\, \mathrm{d}x, \tag{2.5}$$

and note the induced norm,

$$\left\| (u,v)^T \right\| = \sqrt{\left\langle (u,v)^T, (u,v)^T \right\rangle_{\mathcal{H}}}. \tag{2.6}$$

The function space $\mathcal{H}$ equipped with (2.5) is a Hilbert space. From here on, we will omit the subscript in writing the inner product (2.5), because the use of it is never ambiguous. In the case $\mathcal{L} = \Delta$ on $\Omega = (0,1)$ and with homogeneous Dirichlet BCs, we have $\mathcal{H} = L^2(0,1) \times L^2(0,1)$ and the inner product and norm are standard, see Section 2.2.

From the assumptions on $\mathcal{L}$, we can formulate the following proposition.

Proposition 2.1. *The eigenvalues determining linear stability of the trivial state $(U,V) = (0,0)$ of system (1.3) partition into two distinct sets of eigenvalues with asymptotically different interspacing. The eigenvalues $\{\mu_k\}_{k\in\mathbb{N}}$ are $\mathcal{O}(\varepsilon)$-interspaced, while the remaining eigenvalues $\{\lambda_k\}_{k\in\mathbb{N}}$ are $\mathcal{O}(1)$-interspaced. Assuming $\alpha, \gamma \neq -\nu_k$, for all $k \in \mathbb{N}$, asymptotically many eigenvalues $\{\mu_k\}_{k\in\mathbb{N}}$ and $\{\lambda_k\}_{k\in\mathbb{N}}$ are $\mathcal{O}(\varepsilon)$ and $\mathcal{O}(1)$, respectively. The eigenvalues and the associated normalized eigenfunctions are*

$$\left\{ \mu_k = -\varepsilon M_k = \varepsilon(\gamma + \nu_k), \quad s_k = \phi_k(x) \begin{pmatrix} 0 \\ 1 \end{pmatrix} \right\}_{k\geq 1}, \tag{2.7}$$

and

$$\left\{ \lambda_k = \alpha + \nu_k, \qquad \sigma_k = \frac{\phi_k(x)}{\sqrt{1 + D_k^2}} \begin{pmatrix} 1 \\ D_k \end{pmatrix} \right\}_{k\geq 1}, \tag{2.8}$$

where

$$D_k = \frac{\varepsilon\beta}{\nu_k(1-\varepsilon) + \alpha - \varepsilon\gamma} = \frac{\varepsilon\beta}{\lambda_k - \mu_k}. \tag{2.9}$$

This proposition is proved below. Note that D_k is well-defined under our assumptions that α, γ stay away from $-\nu_k$. The fact that all eigenfunctions can be decomposed as scalar x-dependent functions and a constant vector is noteworthy and becomes fairly important in our analysis. It is due to the same differential operator $\mathcal{L}$ appearing in the U- and the V-equation, both with the same BCs.

The first $N\mu$-eigenvalues are $\mathcal{O}(\varepsilon)$ and $\mathcal{O}(\varepsilon)$-interspaced, see (2.7). Therefore, we call this part of the spectrum the *small spectrum*. Accordingly, $\{\lambda_k\}_{k\in\mathbb{N}}$ is called the *large spectrum*, which has $\mathcal{O}(1)$-interspacing. The threshold values for μ_1 and λ_1 to become unstable are the $\mathcal{O}(1)$, fixed values $\gamma = -\nu_1$ and $\alpha = -\nu_1$. Initially, we keep $\gamma < -\nu_1$ fixed, so that the small spectrum is stable. The parameter α is used as a bifurcation parameter and determines the stability of $(0,0)$. We define

$$\alpha_T = -\nu_1, \tag{2.10}$$

where T stands for 'transcritical'. The primary eigenvalue of the large spectrum, λ_1, is unstable for $\alpha > \alpha_T$. Note that the destabilization value for the small spectrum could also be described as $\gamma_T = -\nu_1$, so that the primary eigenvalue of the small spectrum, μ_1, is unstable for $\gamma > \gamma_T$. By setting $\mu_k = -\varepsilon M_k$, we make the asymptotic magnitude of the small spectrum explicit, and because $\gamma < \gamma_T$ almost everywhere in this article, we also make the sign explicit.

Proof of Proposition 2.1. This proof uses assumptions A1–A3 on $\mathcal{L}$ and on the BCs, as well as the solutions of the associated spectral problem (2.3). Due to the triangular structure of $\mathcal{DT}$, one set of eigenvectors is of the form

$$s_k(x) := \begin{pmatrix} 0 \\ \zeta_k(x) \end{pmatrix}. \tag{2.11}$$

The eigenvalues corresponding to s_k are μ_k. Eq. (2.2a) is satisfied trivially and (2.2b) yields a scalar, self-adjoint spectral problem,

$$(\mu_k - \varepsilon\gamma)\zeta_k = \varepsilon\mathcal{L}\zeta_k. \tag{2.12}$$

We can identify (2.12) as the scalar spectral problem (2.3) with a linear shift. Solutions of (2.12) are therefore the eigenfunctions $\zeta_k(x) = \phi_k(x)$, and the corresponding eigenvalues $\mu_k = \varepsilon(\gamma + \nu_k)$ immediately follow. Normalizing $s_k(x)$ under the norm (2.6) yields (2.7).

To derive the second set of eigenvalues and eigenfunctions, we write the eigenfunctions as

$$\sigma_k(x) = \begin{pmatrix} w_k(x) \\ y_k(x) \end{pmatrix}. \tag{2.13}$$

Substitution of (2.13) into (2.2a) yields an ODE for $w(x)$ that decouples from $y(x)$. In this ODE, the scalar problem (2.3) can again be identified, so that,

$$\lambda_k = \alpha + \nu_k \quad \text{and} \quad w_k(x) = c_{1,k}\phi_k(x),$$

with $c_{1,k} \in \mathbb{R}$, a constant depending on the value of ν_k. From this, equation (2.2b) becomes an ODE driven by the inhomogeneity $\varepsilon\beta\phi_k(x)$,

$$\lambda_k y_k(x) = \varepsilon\mathcal{L}y_k(x) + \varepsilon\beta c_{1,k}\phi_k(x) + \varepsilon\gamma y_k(x), \tag{2.14}$$

implying

$$y_k(x) = c_{2,k}\phi_k(x), \quad \text{for some } c_{2,k} \in \mathbb{R}.$$

Substituting into (2.14), we obtain

$$(\alpha+\nu_k)c_{2,k}\phi_k = \varepsilon c_{2,k}\mathcal{L}\phi_k + \varepsilon\beta c_{1,k}\phi_k + \varepsilon\gamma c_{2,k}\phi_k = \varepsilon\left[c_{2,k}\nu_k + \beta c_{1,k} + \gamma c_{2,k}\right]\phi_k,$$

so that we find

$$c_{2,k} = \frac{\varepsilon\beta}{\alpha+(1-\varepsilon)\nu_k-\varepsilon\gamma}c_{1,k} = \frac{\varepsilon\beta}{\lambda_k-\mu_k}c_{1,k}.$$

The constant $c_{1,k}$ is uniquely defined by normalizing σ_k. We then obtain the second set of eigenvalues and eigenfunctions (2.8). □

2.2. Example: a reaction–diffusion system

We illustrate our approach by setting $\mathcal{L}=\Delta$ and $\Omega=(0,1)$, so that $\mathcal{H}=L^2_0(0,1)$. Hence, we study the reaction–diffusion system,

$$\begin{cases} U_t = U_{xx} + \alpha U + F(U,V), \\ V_t = \varepsilon\left[V_{xx} + \beta U + \gamma V + G(U,V)\right]. \end{cases} \tag{2.15}$$

We assume homogeneous Dirichlet BCs, $U(0)=U(1)=V(0)=V(1)=0$. The eigenvalue–eigenfunction pairs for the 1-dimensional Laplacian ∂_{xx} on the unit interval are

$$\nu_k = -k^2\pi^2 \quad \text{and} \quad \phi_k(x)=\sin(k\pi x), \quad \text{with } k\in\mathbb{N}. \tag{2.16}$$

Normalized under the norm of $L^2(0,1)$, the eigenfunctions form an orthonormal set in $L^2(0,1)$,

$$\begin{aligned} &\left\{\mu_k=\varepsilon(\gamma-k^2\pi^2),\quad s_k(x)=\sqrt{2}\sin(k\pi x)\begin{pmatrix}0\\1\end{pmatrix}\right\}_{k\geq1}, \\ &\left\{\lambda_k=\alpha-k^2\pi^2,\quad \sigma_k(x)=\frac{\sqrt{2}\sin(k\pi x)}{\sqrt{1+D_k^2}}\begin{pmatrix}1\\D_k\end{pmatrix}\right\}_{k\geq1}, \end{aligned} \tag{2.17}$$

where D_k is defined as in (2.9). In this case, $\alpha_T=\gamma_T=\pi^2$, so when $\gamma<\gamma_T$, the small spectrum is stable. This example is used extensively in numerical simulations in Sections 4.2 and 5.2, but in the next sections we again turn to an abstract $\mathcal{L}$.

3. Emergence of a small pattern

In Section 2, we have obtained explicit control over the spectrum of (1.3) corresponding to the trivial background state $(U,V)=(0,0)$. In the current section, we set $\lambda_1=r\varepsilon^\sigma$, with $r>0$ and $\sigma>1$, and trace the onset of pattern formation as the background state destabilizes. Since $|\lambda_1|\ll\min_{m,n}\{\mu_m,\lambda_n\}$, there exists a spectral gap and the flow on a center manifold governs the nonlinear dynamics of small initial conditions. As mentioned in the Introduction, we operate slightly different from the textbook center manifold reduction approach but can recover equivalent results — a transcritical bifurcation and the corresponding flow on a 1-dimensional center manifold.

3.1. Fourier expansion and amplitude ODEs

Consider again the function space $\mathcal{H}$ defined in (2.4). By construction, the eigenfunctions s_k and σ_k, see (2.7) and (2.8), form a basis for it. In contrast to [7], we choose to *not* work with the eigenbasis but with

$$\left\{e_k := \begin{pmatrix}\phi_k\\0\end{pmatrix},\quad e_k' := \begin{pmatrix}0\\\phi_k\end{pmatrix}\right\}_{k\in\mathbb{N}}. \tag{3.1}$$

Although this will lead to linear coupling between modes, it will render the amplitude ODEs more amenable to analysis by eliminating many nonlinearities. Since $\mathcal{L}$ is self-adjoint, this basis is orthonormal:

- $\langle e_l, e_m\rangle = \langle e_l', e_m'\rangle = \delta_{lm}$, for all $l,m\in\mathbb{N}$;
- $\langle e_l, e_m'\rangle = 0$, for all $l,m\in\mathbb{N}$;
- $\|e_l\| = \|e_l'\| = 1$, for all $l\in\mathbb{N}$.

Here, $\langle\cdot,\cdot\rangle$ and $\|\cdot\|$ denote the inner product and norm on $\mathcal{H}$ as defined in (2.5) and (2.6). With this basis for $\mathcal{H}$, we can decompose U and V as

$$\begin{pmatrix}U\\V\end{pmatrix} = \sum_{l\geq1}A_l(t)e_l + B_l(t)e_l' = \sum_{l\geq1}\phi_l(x)\begin{pmatrix}A_l(t)\\B_l(t)\end{pmatrix}. \tag{3.2}$$

In the context of our reaction–diffusion example (2.15), (3.2) amounts to Fourier sine series for U and V. The coefficients A_l and B_l are called *amplitudes* corresponding to e_l and e_l', respectively, and measure the projection of the solution $(U,V)^{\mathrm{T}}$ along the corresponding eigenspace. If that solution is known, then the orthonormality relations yield simple formulas for these amplitudes:

$$A_l = \left\langle\begin{pmatrix}U\\V\end{pmatrix}, e_l\right\rangle, \qquad B_l = \left\langle\begin{pmatrix}U\\V\end{pmatrix}, e_l'\right\rangle.$$

Because each ϕ_l is an eigenfunction of the operator $\mathcal{L}$, substitution of (3.2) into (1.3) yields

$$\sum_{l\geq1}\begin{pmatrix}\dot A_l\\\dot B_l\end{pmatrix}\phi_l = \sum_{l\geq1}\begin{pmatrix}\lambda_l & 0\\ \varepsilon\beta & \mu_l\end{pmatrix}\begin{pmatrix}A_l\\B_l\end{pmatrix}\phi_l + \mathcal{N}(U,V), \tag{3.3}$$

cf. (2.2a)–(2.2b). Here, the dot $\dot{}$ denotes differentiation with respect to t. We Taylor-expand the nonlinearity $\mathcal{N}=(F,\varepsilon G)^{\mathrm{T}}$ as

$$\begin{aligned} F(U,V) &= F_{20}U^2 + F_{11}UV + F_{02}V^2 + \mathcal{O}(\|U^2+V^2\|^{\frac{3}{2}}), \\ G(U,V) &= G_{20}U^2 + G_{11}UV + G_{02}V^2 + \mathcal{O}(\|U^2+V^2\|^{\frac{3}{2}}), \end{aligned} \tag{3.4}$$

where $\mathcal{O}(\|U^2+V^2\|^{\frac{3}{2}})$ denotes cubic and higher order terms. Upon substituting (3.2) into these expressions, the nonlinearity becomes

$$\mathcal{N}(U,V) = \sum_{l,m\geq1}\phi_l\phi_m\begin{pmatrix}F_{20}A_lA_m + F_{11}A_lB_m + F_{02}B_lB_m \\ \varepsilon\left(G_{20}A_lA_m + G_{11}A_lB_m + G_{02}B_lB_m\right)\end{pmatrix} + \mathcal{O}(\|U^2+V^2\|^{\frac{3}{2}}), \tag{3.5}$$

which can now be substituted back into (3.3). Note that the quadratic terms $\phi_l\phi_m$ must also be projected onto $\{\phi_k\}_{k\geq1}$,

$$\phi_l\phi_m = \sum_{k\geq1}C_{klm}\phi_k, \quad \text{with } C_{klm} = \int_\Omega \phi_k\phi_l\phi_m\,\mathrm{d}x, \tag{3.6}$$

where C_{klm} is invariant under index permutations. In the case $\mathcal{L}=\Delta$, $\Omega=(0,1)$ and with Dirichlet BCs, for example, $C_{111}=8\sqrt{2}/(3\pi)$ and $C_{klm}=0$ if $k+l+m$ is even. The resulting system is reducible to an infinite-dimensional system of ODEs for A_k and B_k by taking the inner product with e_k and e_k', respectively. One thus obtains a pair of coupled ODEs per $k\in\mathbb{N}$:

$$\begin{cases} \dot A_k = \lambda_kA_k + \displaystyle\sum_{l,m\geq1}C_{klm}\left(F_{20}A_lA_m + F_{11}A_lB_m + F_{02}B_lB_m\right), \\ \dot B_k = -\varepsilon M_kB_k + \varepsilon\beta A_k \\ \qquad + \varepsilon\displaystyle\sum_{l,m\geq1}C_{klm}\left(G_{20}A_lA_m + G_{11}A_lB_m + G_{02}B_lB_m\right), \end{cases} \tag{3.7}$$

up to cubic corrections. Note that there is now also *linear coupling* between A_k and B_k, reflecting the fact that $\{e_k,e_k'\}_{k\geq1}$ is not an eigenbasis of $\mathcal{DT}$.

3.2. The classical center manifold reduction

As discussed in the Introduction, center manifold reduction (CMR) can be used to reduce the flow of a system close to bifurcation, provided that there is a spectral gap between the bifurcating eigenvalues and the other (stable) eigenvalues. To that effect, we rescale

$$\alpha = \alpha_T + r\varepsilon^\sigma, \quad \text{with } r > 0 \text{ and } \sigma > 1, \text{ so that } \lambda_1 = r\varepsilon^\sigma; \tag{3.8}$$

this positions us just beyond destabilization of $(U, V) = (0, 0)$. As we have already remarked, the spectral gap condition is satisfied in this regime; recall Fig. 1.1. The results in this section are therefore equivalent to CMR, see [1–3].

We trace the onset of patterns emerging from a trivial background state, so we expect all amplitudes to be small. To reflect this, we scale all amplitudes by means of

$$\begin{aligned} A_1(t) &= \varepsilon^{\sigma_1} a_1(t), \\ A_k(t) &= \varepsilon^{\sigma_U} a_k(t), \quad k \in \mathbb{N}_{\geq 2}, \\ B_k(t) &= \varepsilon^{\sigma_V} b_k(t), \quad k \in \mathbb{N}, \end{aligned} \tag{3.9}$$

with $\sigma_1 < \sigma_U$. We assumed here that the primary amplitude A_1 is asymptotically larger than all other amplitudes, because it corresponds to the bifurcating eigenvalue. The powers $\sigma_1, \sigma_U, \sigma_V$ are positive and will be determined in terms of σ in the forthcoming analysis. Substituting the rescaled amplitudes into system (3.7) yields,

$$\begin{aligned} \varepsilon^{\sigma_1}\dot{a}_1 &= r\varepsilon^{\sigma_1+\sigma} a_1 + \varepsilon^{2\sigma_1} C_{111} F_{20} a_1^2 + \varepsilon^{\sigma_1+\sigma_V} \sum_{m\geq 1} C_{11m} F_{11} a_1 b_m \\ &\quad + \varepsilon^{2\sigma_V} \sum_{l,m\geq 1} C_{1lm} F_{02} b_l b_m + \mathcal{O}(\varepsilon^{\sigma_1+\sigma_U}, \varepsilon^{\sigma_V+\sigma_U}), \\ \varepsilon^{\sigma_U}\dot{a}_k &= \varepsilon^{\sigma_U} \lambda_k a_k + \varepsilon^{2\sigma_1} C_{k11} F_{20} a_1^2 + \varepsilon^{\sigma_1+\sigma_V} \sum_{m\geq 1} C_{k1m} F_{11} a_1 b_m, \\ &\quad + \varepsilon^{2\sigma_V} \sum_{l,m\geq 1} F_{02} C_{klm} b_l b_m + \mathcal{O}(\varepsilon^{\sigma_1+\sigma_U}, \varepsilon^{\sigma_V+\sigma_U}), \\ \varepsilon^{\sigma_V}\dot{b}_1 &= -\varepsilon^{1+\sigma_V} M_1 b_1 + \varepsilon^{1+\sigma_1} \beta a_1 \\ &\quad + \mathcal{O}(\varepsilon^{1+2\sigma_1}, \varepsilon^{1+\sigma_1+\sigma_V}, \varepsilon^{1+2\sigma_V}), \\ \varepsilon^{\sigma_V}\dot{b}_k &= -\varepsilon^{1+\sigma_V} M_k b_k + \varepsilon^{1+\sigma_U} \beta a_k \\ &\quad + \mathcal{O}(\varepsilon^{1+2\sigma_1}, \varepsilon^{1+\sigma_1+\sigma_V}, \varepsilon^{1+2\sigma_V}), \end{aligned} \tag{3.10}$$

with the higher order corrections originating from the nonlinear terms in (3.7). The *principle* of *least degeneracy* or of *significant degeneration* [14,15] suggests that $\sigma = \sigma_1 = \sigma_V$, that $\sigma_U = 2\sigma$ and the rescaling of time $\tau = \varepsilon^\sigma t$. Denoting differentiation with respect to τ by $'$, we find

$$\begin{aligned} a_1' &= r a_1 + C_{111} F_{20} a_1^2 + F_{11} a_1 \sum_{m\geq 1} C_{11m} b_m \\ &\quad + F_{02} \sum_{l,m\geq 1} C_{1lm} b_l b_m + \mathcal{O}(\varepsilon^\sigma), \\ \varepsilon^\sigma a_k' &= \lambda_k a_k + C_{k11} F_{20} a_1^2 + F_{11} a_1 \sum_{m\geq 1} C_{k1m} b_m \\ &\quad + F_{02} \sum_{l,m\geq 1} C_{klm} b_l b_m + \mathcal{O}(\varepsilon^\sigma), \\ \varepsilon^{\sigma-1} b_1' &= -M_1 b_1 + \beta a_1 + \mathcal{O}(\varepsilon^\sigma), \\ \varepsilon^{\sigma-1} b_k' &= -M_k b_k + \mathcal{O}(\varepsilon^\sigma). \end{aligned} \tag{3.11}$$

For $\sigma > 1$, the left hand side of all ODEs except the first one is of higher order, compared to their linear terms. This reflects the disparity between the $\mathcal{O}(\varepsilon^\sigma)$ eigenvalue λ_1 and all other eigenvalues, which are at least $\mathcal{O}(\varepsilon)$. It ensures that the long-term, leading order behavior of the corresponding modes are described by algebraic relations — *slaving relations* — because the left-hand sides become higher order compared to the linear terms. The corresponding amplitudes are said to be *slaved* to a_1, leaving this as the only *dynamic* amplitude and the behavior of (3.11) completely determined by it. Here, the slaving relations assume the form

$$\begin{aligned} b_1 &= \frac{\beta}{M_1} a_1 + \mathcal{O}(\varepsilon^{\sigma-1}), \\ b_k &= 0 + \mathcal{O}(\varepsilon^{\sigma-1}), \\ a_k &= -\frac{C_{k11} H}{\lambda_k} a_1^2 + \mathcal{O}(\varepsilon^{\sigma-1}), \end{aligned} \tag{3.12}$$

where, with a slight abuse of notation, we write

$$H = F_{20} + \frac{F_{11}\beta}{M_1} + \frac{F_{02}\beta^2}{M_1^2}. \tag{3.13}$$

The ODE describing the evolution of a_1 on the center manifold is

$$a_1' = r a_1 + H C_{111} a_1^2 + \mathcal{O}(\varepsilon^{\sigma-1}), \tag{3.14}$$

obtained by substituting (3.12) into (3.11). At this point, we have recaptured the classical center manifold reduction results. The center manifold is 1-dimensional and described by the slaving relations, while the evolution on it is governed by the single ODE for a_1 above. The trivial pattern $(U, V) = (0, 0)$ corresponds to the trivial steady state $a_1 \equiv 0$, and there also exists a nontrivial steady state solution,

$$a_1^* = -\frac{r}{C_{111} H}. \tag{3.15}$$

This state indicates the onset of a nontrivial pattern, because the two steady states exchange stability at $r = 0$ through a transcritical bifurcation. As long as $\sigma > 1$, (3.14) exhibits no other bifurcations in a neighborhood of $(U, V) = (0, 0)$.

Theorem 3.1. *The trivial state $(U, V) = (0, 0)$ of system (1.3) undergoes a transcritical bifurcation at $\alpha = \alpha_T$. For $\alpha = \alpha_T + r\varepsilon^\sigma$ with $\sigma > 1$, $r > 0$ and $\gamma < \gamma_T$, the nontrivial, stationary, attracting pattern branching off this trivial state is approximated by*

$$\begin{pmatrix} U \\ V \end{pmatrix} = \varepsilon^\sigma \left[-\frac{r}{C_{111} H} \begin{pmatrix} 1 \\ \beta/M_1 \end{pmatrix} \phi_1(x) + \mathcal{O}(\varepsilon^{\sigma-1}) \right]. \tag{3.16}$$

This result is derived by combining (3.15) and the slaving relations (3.12) with the original expansion (3.2). It also follows from a standard application of center manifold reduction, and therefore we refer to [1–3] for a full proof.

4. Evolution of the small pattern outside the CMR regime

The dichotomy $\sigma > 1$ versus $\sigma = 1$ arises naturally in system (3.11). Indeed, as $\sigma \downarrow 1$, the spectral gap between a_1 and the b_k-amplitudes disappears, although the assumed disparity between the large eigenvalues maintains the slaving relations for the a_k-amplitudes with $k \geq 2$. Those b_k-amplitudes naturally remain linearly stable, but they now evolve in the same timescale as a_1. As a result, (3.11) does not necessarily support an exponentially attracting, 1-dimensional center manifold anymore.

Below, we use the spectrum of the background state and (3.11) to track the evolution of the small pattern (3.16) emerging from that state well into the regime $\sigma = 1$. We first show that the pattern (conditionally) undergoes a destabilizing Hopf bifurcation at a value $\alpha_H > \alpha_T$ for α, through which emerges a small, stable, temporally oscillatory pattern; see Section 4.1. As α increases even further, numerical work show the amplitude and period of the oscillation to increase all the way to a homoclinic bifurcation, at which the oscillatory pattern disappears. Past that α-value, small initial conditions grow unboundedly (in the scaled setting), see Section 4.2; this bounds the span of our analysis explicitly.

4.1. Beyond classical CMR: a Hopf bifurcation

Setting $\sigma = 1$ in (3.11) and retaining the dynamic equations for the b_k-modes, we obtain, up to $\mathcal{O}(\varepsilon)$ corrections,

$$\begin{cases} a_1' = ra_1 + C_{111}F_{20}a_1^2 + F_{11}a_1\sum_{n\geq 1} C_{1n1}b_n \\ \qquad + \sum_{m,n\geq 1} C_{mn1}F_{02}b_m b_n, & \text{(a)} \\ b_1' = -M_1 b_1 + \beta a_1, & \text{(b)} \\ b_k' = -M_k b_k, \quad \text{where } k \geq 2. & \text{(c)} \end{cases} \tag{4.1}$$

The amplitudes a_k with $k \geq 2$ remain slaved. However, since all b_k-modes are now dynamic, each a_k is controlled by both the a_1- and the b_k-modes,

$$a_k = -\frac{C_{11k}F_{20}a_1^2 + F_{11}a_1\sum_{n\geq 1} C_{1nk}b_n + \sum_{m,n\geq 1} C_{mnk}F_{02}b_m b_n}{\lambda_k}.$$

In the terminology of center manifold reduction (CMR), one could say that the center manifold dimension has become infinite or, at least, that it cannot be bounded uniformly as $\varepsilon \downarrow 0$ (asymptotically large). Analysis of an infinite-dimensional ODE system is a priori nontrivial. Here, however, all but one — a_1' — of the equations are linear and all but two — a_1' and b_1' — decouple, see also Remark 4.2. Moreover, the ODEs for b_k with $k \geq 2$, see (4.1)(c), imply exponential decay of those modes at rates increasing with k. In the long term, therefore, $b_k = \mathcal{O}(\varepsilon)$ for all $k \geq 2$, see again Remark 4.2, and the evolution of the pattern is controlled by the planar system

$$\begin{cases} a_1' = ra_1 + C_{111}\left(F_{20}a_1^2 + F_{11}a_1b_1 + F_{02}b_1^2\right) + \mathcal{O}(\varepsilon), \\ b_1' = -M_1 b_1 + \beta a_1 + \mathcal{O}(\varepsilon), \end{cases} \tag{4.2}$$

together with the slaving relations

$$a_k = -\frac{C_{11k}}{\lambda_k}\left[F_{20}a_1^2 + F_{11}a_1b_1 + F_{02}b_1^2\right] + \mathcal{O}(\varepsilon),$$
$$b_k = \mathcal{O}(\varepsilon), \quad k \geq 2.$$

The reduced system (4.2) admits two equilibria, namely the zero solution corresponding to the trivial state and the continuation of the pattern (3.16) in this regime,

$$S^*(r) := \left(-\frac{r}{C_{111}H}, -\frac{\beta r}{M_1 C_{111}H}\right); \tag{4.3}$$

recall definition (3.13) for H. The Jacobian of the trivial state has eigenvalues $\Lambda_1 = r$ and $\Lambda_2 = -M_1$, and thus the state changes from stable node to saddle at the transcritical bifurcation ($r = 0$). The stability of S^* is determined by the Jacobian corresponding to (4.2),

$$J(S^*) = \begin{pmatrix} \frac{r}{H}(H - J_1) & -\frac{r}{H}J_2 \\ \beta & -M_1 \end{pmatrix},$$
$$\text{with } J_1 = 2F_{20} + \frac{\beta F_{11}}{M_1} \quad \text{and} \quad J_2 = F_{11} + 2\frac{\beta F_{02}}{M_1}. \tag{4.4}$$

One of its eigenvalues becomes zero if and only if $r = 0$, as expected because of the transcritical bifurcation, (see Appendix). The branch $S^*(r)$ may further lose stability through a Hopf bifurcation, where limit cycles (periodic amplitudes) are born; this occurs if the eigenvalues form a complex pair crossing the imaginary axis. A straightforward computation gives conditions on r for which the eigenvalues of $J(S^*)$ are purely imaginary complex conjugates:

$$r_H = \frac{HM_1}{H - J_1} \quad \text{and} \quad r_H > 0. \tag{4.5}$$

If $r_H < 0$ instead, S^* remains a stable point for all positive $\mathcal{O}(1)$ values of r. However, we refrain from investigating the fate of S^* in the case that it does not undergo a Hopf bifurcation. If $r_H > 0$ and $H - J_1 \neq 0$, then a Hopf bifurcation takes place. The degeneracy condition ensuring that the eigenvalues pass the imaginary axis with nonzero speed is automatically satisfied if $r_H > 0$ [16]. Straightforward computations determine the criticality of the bifurcation [16]. Defining

$$L = (H + r_H F_{20})(2M_1F_{20} + F_{11}\beta), \tag{4.6}$$

we obtain that the Hopf bifurcation is supercritical if $L < 0$ and subcritical if $L > 0$. We refer the reader to Appendix for the full derivation of this expression. Our results so far, concerning the evolutionary system (1.3), are summarized in the following proposition.

Claim 4.1. *In PDE-systems of the class (1.3), the trivial solution $(U, V) = (0, 0)$, undergoes a transcritical bifurcation as α passes through $\alpha_T = -\nu_1$. When the trivial solution loses stability, the nontrivial branch becomes stable and, under the condition that $r_H > 0$, undergoes a Hopf bifurcation as α increases to*

$$\alpha_H = \frac{HM_1}{H - J_1}\varepsilon - \nu_1.$$

Neither a rigorous proof of this proposition nor validation of the asymptotics are foci of this presentation, and they are deferred to future work. The formal work resulting in Claim 4.1 establishes that, as long as $r_H > 0$ and $L < 0$, the bifurcating stationary pattern (3.16) starts oscillating periodically in time for parameters $\mathcal{O}(\varepsilon)$ close to the first transcritical bifurcation. As in the case of the phytoplankton-nutrient model (1.1), this behavior is confirmed by direct simulations of the full PDE model; see next section.

Remark 4.1. In system (4.1), the dynamics of the b_k-modes is governed by ODEs. However, together the b_k-modes represent the leading order original PDE for V, see (1.3), through transformation (3.2). System (4.1) can therefore also be regarded as an ODE (equation (4.1)(a)) coupled to a PDE (albeit in amplitude form, (4.1)(b)–(c)). We can reconstruct the PDE to which equation (4.1)(a) is coupled by writing $V(x, t) = \varepsilon v(x, t)$ and using the correct timescale $\tau = \varepsilon t$ in (1.3). The PDE for v then becomes

$$v_\tau = \mathcal{L}v + \gamma v + \beta a_1(\tau)\phi_1(x) + \mathcal{O}(\varepsilon). \tag{4.7}$$

System (4.1) is thus equivalent to (4.1)(a) coupled to the inhomogeneous, linear PDE (4.7). The analogue of this compact version of system (1.3) is heavily used in [8]. Note also that all b_k-terms appearing in (4.1)(a) can in principle be expressed into nonlocal terms of v. We did not work with this representation of the dynamics beyond classical CMR, because of being able to reduce (4.1) to the planar system (4.2).

Remark 4.2. The distinct decoupling between the active b_1-mode and the exponentially decaying b_k-modes ($k \geq 2$) in the extended center manifold reduction (ECMR) system (4.1) can be traced back to our assumptions on the structure of the basic system (1.3) and its BCs. Since the fast (U) and slow (V) eigenvalue problems are governed by the same operator $\mathcal{L}$ subject to the same BCs, we can employ the Fourier decomposition (3.2) based on the same *scalar* eigenfunctions $\phi_k(x)$ for both the U- and the V-components. In a more general setting — e.g., when the operator and BCs for U differ from those for V — the fast and slow eigenvalue problems do not admit a set of eigenfunctions expressible in terms of the same scalar function. As a consequence, the *leading order* terms in the (beyond CMR) ODEs for b_k may employ the unstable a_1-mode; in that case, a direct decoupling of the form (4.1) is not ascertained. We encounter that in the phytoplankton-nutrient model (1.1) studied in [5,7,6,8]. It has, nevertheless, been shown in [7] that, also for (1.1), the full system behavior

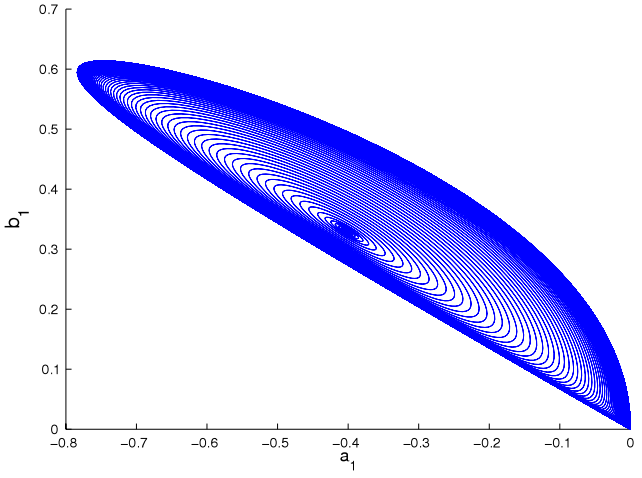

Fig. 4.1. A continuation of the attracting limit cycle in system (4.2) that originates at the Hopf bifurcation. The horizontal and vertical axes correspond to a_1 and b_1, respectively. The parameter values are $\beta = -4, \gamma = 5, F_{20} = -2, F_{11} = 5, F_{02} = 12$, so that $r_H > 0$ and $L < 0$. The supercritical Hopf bifurcation occurs at $r_H \approx 0.9596$. The limit cycles accumulate at $r \approx 1.0524$, at which point the period tends to infinity. This indicates the existence of an orbit homoclinic to the trivial state $(0, 0)$. As r increases beyond $r \approx 1.0524$, orbits grow unboundedly.

is essentially 2-dimensional. The transcritical bifurcation in (1.1) is also followed by a Hopf destabilization. Although we do not consider the more general case, (1.2), here, we expect it to behave similarly to systems (1.1) and (1.3): essentially 2-dimensional dynamics, beyond the classical CMR, which may contain a Hopf bifurcation. The difference between the present, most transparent case (1.3) and the more general (1.2) is expected to mostly be a matter of linear algebra.

4.2. Beyond the Hopf: a homoclinic bifurcation

Having successfully tracked the pattern into an $\mathcal{O}(\varepsilon)$ regime beyond the transcritical bifurcation, the question arises whether the ECMR system (4.2) can possibly capture tertiary bifurcations for $\alpha > \alpha_H$. It turns out that, unfortunately, we cannot in general expect (E)CMR to capture the full system dynamics for $r > r_H$. As we will find out, even small initial conditions are no more trapped in a neighborhood of the manifold.

First, we select parameter values ensuring the existence of a supercritical Hopf bifurcation and then trace the stable limit cycle emerging through it. We do not attempt to follow the oscillatory pattern analytically but rely, instead, on numerical ODE continuation toolbox MatCont to do just that [17]. The first outcome is Fig. 4.1, where we have plotted the limit cycle born at α_H for increasing r (or, equivalently, α; recall (3.8)). Note carefully that these plots correspond to the *reduced*, planar system (4.2) and not to the full PDE model; also, that we have overlaid the limit cycles corresponding to several r-values — this is not a single trajectory. As r increases from r_H, the period of the limit cycle tends to infinity while it accumulates to a homoclinic orbit; this occurs at a well-defined, finite value r_{Hom}. As Fig. 4.1 shows, that orbit is homoclinic to the trivial state $(a_1, b_1) = (0, 0)$. Increasing r beyond r_{Hom} leads amplitudes to grow unboundedly, rendering our asymptotic analysis invalid; indeed, the assumption on the asymptotic magnitude of A_1 and B_1 is then violated, see (3.9).

MATLAB simulations show that the full system (1.3) exhibits similar behavior and has a periodically oscillating spatial structure as attractor. Moreover, the periodic patterns also seem to merge with a homoclinic structure as r increases, see Fig. 4.2 where we plot the amplitudes $a_1(\tau)$ and $b_1(\tau)$. Motivated by these observations, we formulate a conjecture concerning the stability of the nontrivial steady state.

Conjecture 4.2. *Let $r_H > 0$ and assume that the Hopf bifurcation that (4.2) undergoes is supercritical: $L < 0$, see (4.6). Then, as r increases beyond r_H, the limit cycles grow into a homoclinic orbit at $r = r_{\text{Hom}}$. As r increases beyond that value, all orbits of (4.2) grow unboundedly except for those with initial conditions on the stable manifold of the trivial state $(0, 0)$. Qualitatively, this transition is illustrated in Fig. 4.3.*

Fig. 4.3 contains (hypothetical) phase portraits of a 2-dimensional system as it goes through the transcritical, Hopf and homoclinic bifurcations. These portraits are meant to illustrate qualitatively these transitions, not to correspond to (4.2) for specific parameter values. Note that the scenario laid out in Conjecture 4.2 has a strong similarity to the behavior of systems near a transcritical codimension 2 Bogdanov–Takens bifurcation point — see [18], for instance. Given the structure of (4.2), this is not surprising. There is, however, a subtle but significant difference between (4.2) and a generic unfolding of a (non-semisimple) codimension 2 bifurcation with two zero eigenvalues as that considered in [18]. Specifically, system (4.2) has been obtained under the assumption that amplitudes a_1 and b_1, as well as all parameters, are strictly $\mathcal{O}(1)$. For instance, $|r| \ll 1$ will necessarily bring us back to the classical center manifold reduction case of a transcritical (codimension 1) bifurcation of Section 3.2. Similarly, it is central to our procedure that M_1 is not 'small' — or equivalently that $\mu_1 = \mathcal{O}(\varepsilon)$ but not

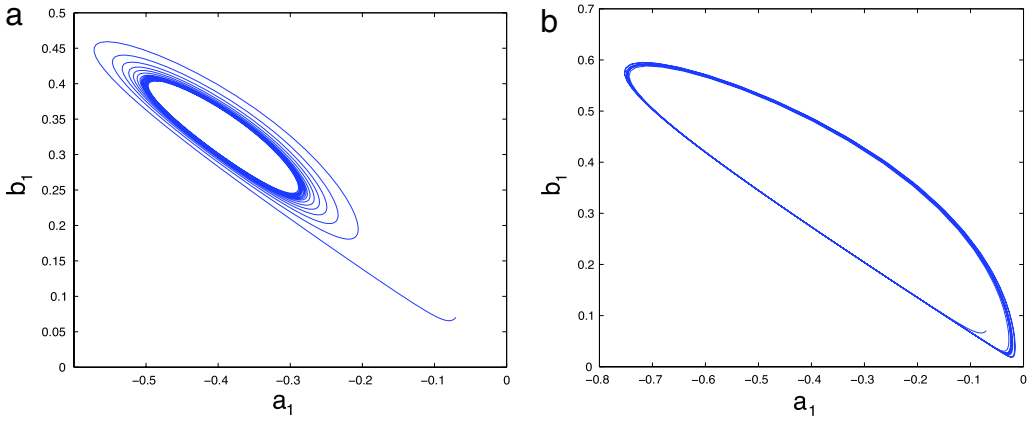

Fig. 4.2. PDE simulations of (1.3) using MATLAB's PDEPE function. Here, $\mathcal{L} = \Delta$ on $\Omega = (0, 1)$ equipped with Dirichlet BCs, and parameters are as in Fig. 4.1 and $G_{20} = 1, G_{11} = G_{02} = 0$. Plotted are the amplitudes a_1 (horizontal axis) and b_1 (vertical axis), obtained by projecting the computed $(U(x, t), V(x, t))$ onto $\phi_1(x)$ and rescaling. (a) An orbit evolving to an attracting limit cycle. Additional parameter values are $r = 1$ and $\varepsilon = 0.05$. The initial conditions are $U(x, 0) = -V(x, 0) = -\varepsilon\phi_1(x)$. (b) A similar simulation for $r = 1.09$. For r slightly larger, the limit cycle connects to the origin and orbits continue to grow (data not shown).

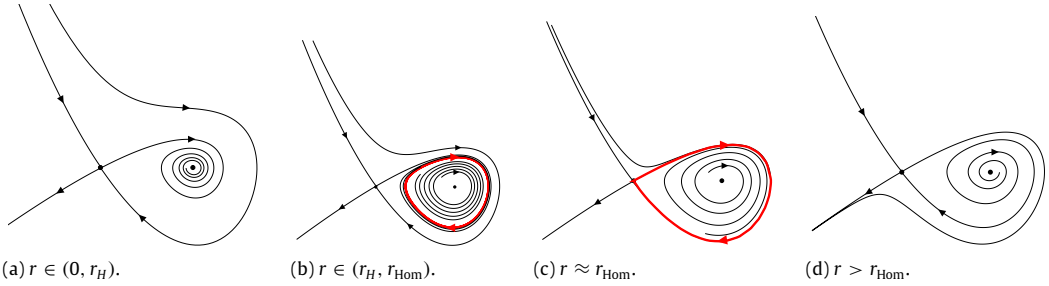

(a) $r \in (0, r_H)$. (b) $r \in (r_H, r_{\text{Hom}})$. (c) $r \approx r_{\text{Hom}}$. (d) $r > r_{\text{Hom}}$.

Fig. 4.3. Qualitative phase portraits illustrating Conjecture 4.2 on the evolution of the stability of the nontrivial steady state S^*. (a) $r \in (\alpha_T, r_H)$; the Hopf bifurcation has not yet occurred, and S^* is a stable focus. (b) $r \in (\alpha_H, r_{\text{Hom}})$; a stable limit cycle has appeared after the Hopf bifurcation, making S^* an unstable focus. (c) $r \approx r_{\text{Hom}}$; the limit cycles have grown into an homoclinic orbit to the origin with attracting initial conditions within its lobe, and S^* is unstable. (d) $r > r_{\text{Hom}}$; now all orbits grow unboundedly, except for the stable manifold of the trivial state.

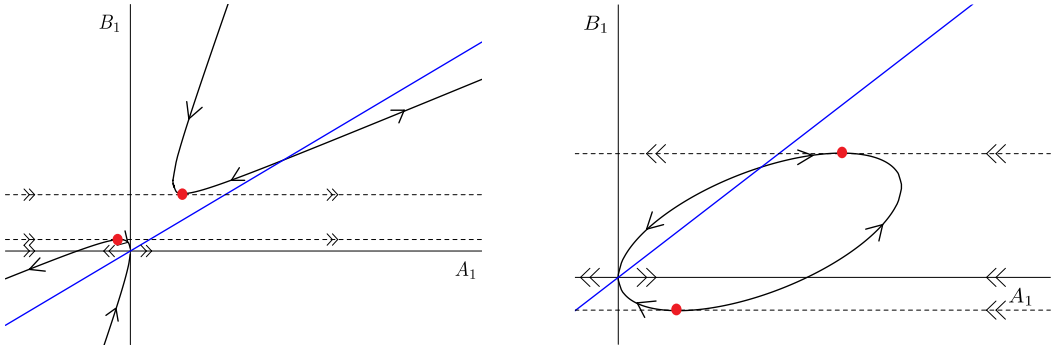

Fig. 4.4. Two possible phase portraits of system (4.8). The red dots mark the folds of the slow manifold. The blue line is $B_1 = \beta A_1/M_1$, and intersections of it with the conic section are steady states. (a) Here, $F_{20} = 1$, $F_{11} = 3$, $F_{02} = 1$ and $\beta = 0.55M_1$, and the conic section is a hyperbola. (b) Here, $F_{20} = -1$, $F_{11} = 2$, $F_{02} = -3$ and $\beta = 0.8M_1$, and the conic section is an ellipse. In both cases, the nontrivial steady state is repelling all initial conditions other than itself. The only orbits that do not grow unboundedly are those with initial conditions on the stable manifold of the trivial steady state.

smaller — as Fig. 1.1 clearly illustrates. Therefore, the conjectured occurrence of the homoclinic bifurcation cannot be deduced from the existence of homoclinic bifurcations near a Bogdanov–Takens point: these are all established by a local analysis zooming into the situation where, in the notation of Eq. (4.2), $|a_1|$, $|b_1|$, r and M_1 are all '*sufficiently small*'. A rigorous proof on the existence of an attracting, extended center manifold as a reduction, is crucial for the validation of our method, but is part of future work.

In fact, the system beyond the center manifold reduction (CMR) obtained in [7] for the phytoplankton — nutrient model (1.1) that inspired the present analysis corresponds to setting $\gamma = 0$ in (1.3), since the small eigenvalues μ_k in (1.1) are parameter-independent and cannot be '*tuned*'. Hence, in the case of (1.1), $M_1 = -\pi^2$ and there is no freedom to consider the case $M_1 \to 0$. Nevertheless, the system beyond CMR obtained in [7] also exhibits the Bogdanov–Takens-like behavior of Conjecture 4.2. This is not surprising: it is natural to assume that bifurcation curves existing in a local limit may be extended globally.

Other than the numerical evidence, we do not provide an analytical proof for the existence of a homoclinic orbit. We will, however, employ geometric singular perturbation theory (GSPT) and Fenichel's theorems to show that, if r increases to be asymptotically large, all solutions of (4.2) indeed blow up [19–21].

We introduce $r = \frac{1}{\delta}$, with $0 < \delta \ll 1$. System (4.2) then becomes singularly perturbed,

$$\begin{cases} a_1' = \dfrac{1}{\delta} a_1 + C_{111}\left(F_{20}a_1^2 + F_{11}a_1b_1 + F_{02}b_1^2\right) + \mathcal{O}(\varepsilon), \\ b_1' = -M_1 b_1 + \beta a_1 + \mathcal{O}(\varepsilon), \end{cases} \tag{4.8}$$

where the prime denotes differentiation with respect to τ. With a slight abuse of notation, we rescale $A_1 = \delta a_1$ and $B_1 = \delta b_1$ to obtain the associated slow system,

$$\begin{cases} \delta A_1' = A_1 + C_{111}\left(F_{20}A_1^2 + F_{11}A_1B_1 + F_{02}B_1^2\right), \\ B_1' = -M_1 B_1 + \beta A_1. \end{cases} \tag{4.9}$$

Rescaling time as $\hat{t} = \frac{1}{\delta}\tau$, we obtain the fast system,

$$\begin{cases} \dfrac{dA_1}{d\hat{t}} = A_1 + C_{111}\left(F_{20}A_1^2 + F_{11}A_1B_1 + F_{02}B_1^2\right), \\ \dfrac{dB_1}{d\hat{t}} = \delta\left(-M_1 B_1 + \beta A_1\right). \end{cases} \tag{4.10}$$

Using GSPT, we can now conclude the following.

- To leading order in δ, B_1 is constant with respect to the fast dynamics.
- The slow manifold is defined by

$$0 = A_1 + C_{111}\left(F_{20}A_1^2 + F_{11}A_1B_1 + F_{02}B_1^2\right), \tag{4.11}$$

  which is a conic section (ellipse, hyperbola or parabola). This slow manifold is normally hyperbolic, except at the folds where the slope with respect to B_1 is zero.
- The eigenvalues of the nontrivial equilibrium S^* determined from the fast system are

$$\Lambda_1 = \frac{M_1}{r_H} + \delta\frac{r_H J_1}{H} + \mathcal{O}(\delta^2) \quad \text{and} \quad \Lambda_2 = \delta r_H + \mathcal{O}(\delta^2), \tag{4.12}$$

  recall (3.13) and (4.4)–(4.5). In the regime which we consider, $r_H > 0$ and $M_1 > 0$, the equilibrium is a source.

Proposition 4.3. *Let $r_H, M_1 > 0$ and $\beta \neq 0$. If a solution $\Gamma(\tau) = (a_1(\tau), b_1(\tau))$ of system (4.8) is bounded, then it lies on the stable manifold of the trivial steady state:* $\lim_{\tau\to\infty} \Gamma(\tau) = (0, 0)$.

Proof. The proof relies on phase portrait analysis. See Fig. 4.4 for two typical configurations of the phase portrait; the situation is similar for a parabolic slow manifold (case not shown). Now, assume $\Gamma(\tau)$ to be bounded and to solve (4.8) but not to limit to the origin. Without loss of generality, we also assume $\Gamma(0)$ to lie on the

fast plane and not on the slow manifold. Given that Γ is bounded, the fast flow takes it to a branch of the slow manifold. There, the slow flow cannot further direct it to the trivial steady state, by assumption. Hence, it carries it to either of the folds of the slow manifold, where the flow of Γ is more subtle. Since there is no other branch of the slow manifold to pick up Γ, that remains unbounded contradicting our assumptions and completing the proof.

Note that, in the above argument, we have implicitly assumed Γ to stay away from the nontrivial steady state S^*. The linear analysis (4.12) confirming S^* as a source supports this conclusion, as does Fig. 4.4. The same figure, nevertheless, suggests the existence of trajectories limiting to S^*, and thus bounded, when that equilibrium lies at the other side of the folds. This cannot happen in the regime assumed here, $M_1 > 0$ and $r_H > 0$. Indeed, switching occurs at $H - J_1 = 0$ and, in our regime, either $H - J_1 > 0$ or $H - J_1 < 0$: the state remains repelling for all $r_H, M_1 > 0$. □

As a corollary of Proposition 4.3, every solution of (4.8) not intersecting the stable manifold of the trivial state grows unboundedly. Hence, orbits of system (4.2) with asymptotically large r grow unboundedly, unless they intersect the stable manifold of the trivial state.

5. Capturing the onset of low-dimensional chaos with the ECMR

In the previous sections, we have analyzed the onset of patterns arising from a trivial background state in (1.3), finding that it involves a primary (transcritical), a secondary (Hopf) and a tertiary (homoclinic) bifurcation. In this and the next section we demonstrate, first, how a modification in (1.3) creates more complex but equally low-dimensional dynamics and, second, how to track the onset of this dynamics using extended center manifold reduction (ECMR). The first part adds to our ongoing effort to unfold the driver of low-dimensional chaotic dynamics in (1.1); and indeed, our work puts the spotlight on a wide class of PDE systems exhibiting similar phenomena, see (1.2) and its concomitant paper [8]. The second part is meant to further highlight this class as one where analysis *is* possible and onset of chaos *may be* understood analytically, for a large part, through ECMR.

As we discussed in the Introduction, the amplitude system (4.1)(a)–(c) can hardly support more exciting dynamics, as it is essentially 2-dimensional through the action of the nonlinearity εG in (1.3). A straightforward choice is amplifying that nonlinearity to G. Note that this does not affect the linear structure of the system near the trivial state — i.e., $\mathcal{DT}$ and thus also the validity of assumptions A1–A3 — which enabled our analysis in the previous sections. We discuss this modification below, deferring to Section 6 the discussion of codimension 2 bifurcations as possible organizing centers for chaos. We start from (cf. (1.3))

$$\begin{cases} U_t = \mathcal{L}U + \alpha U + F(U,V), \\ V_t = \varepsilon\mathcal{L}V + \varepsilon\beta U + \varepsilon\gamma V + G(x,U,V), \end{cases} \tag{5.1}$$

equipped with suitable BCs, and focus for specificity on nonlinearities G that are locally quadratic in U only. Spatial inhomogeneity, modeled here by an x-dependent G and which is also present in (1.1), will become important in Section 5.2. As we will see, the corresponding amplitude system is now infinite-dimensional, with all b_k-modes *nonlinearly* coupled to a_1. To explore the ramifications of this dramatic increase in dimensionality, we consider a special case in Section 5.2 and recover an essentially 5-dimensional reduced system with chaotic dynamics. We conclude this exploratory piece with simulations of the full PDE system, through which we identify spatio-temporal chaos bearing strong similarities to that of the reduced system.

5.1. New amplitude equations

In this section, we set $G(x,U,V) = G_{20}(x)U^2$ at leading order in (U,V,ε), with G_{20} an arbitrary function. We thus study a modification of (1.3) with an $\mathcal{O}(1)$, quadratic nonlinearity for V,

$$\begin{cases} U_t = \mathcal{L}U + \alpha U + F(U,V), \\ V_t = \varepsilon\mathcal{L}V + \varepsilon\beta U + \varepsilon\gamma V + G_{20}(x)U^2 \\ \qquad + \mathcal{O}\left(\varepsilon UV, \varepsilon V^2, \left\|U^2+V^2\right\|^{3/2}\right); \end{cases} \tag{5.2}$$

the nonlinearity F is as in (3.4). We again equip the system with suitable BCs guaranteeing conditions A1–A3, and we set $\alpha = r\varepsilon^\sigma - \nu_1$ to have $(0,0)$ destabilize at $r = 0$.

The analysis proceeds along the same lines as that of system (1.3) in Sections 3 and 4. Using a Fourier-like decomposition in terms of amplitudes and eigenfunctions for U and V — recall (3.2) — system (5.2) is written as an infinite-dimensional system of ODEs,

$$\begin{aligned} \dot{A}_k &= \lambda_k A_k + \sum_{l,m\geq 1} C_{klm}\left(F_{20}A_lA_m + F_{11}A_lB_m + F_{02}B_lB_m\right), \\ \dot{B}_k &= -\varepsilon M_k B_k + \varepsilon\beta A_k + \sum_{l,m\geq 1} H_{klm}A_lA_m + \mathcal{O}(\varepsilon A_lB_m, \varepsilon B_lB_m). \end{aligned} \tag{5.3}$$

Here, H_{klm} is the projection of $G_{20}\phi_l\phi_m$ onto ϕ_k,

$$H_{klm} = \int_\Omega G_{20}(x)\phi_k(x)\phi_l(x)\phi_m(x)\,\mathrm{d}x; \tag{5.4}$$

note that H_{klm} reduces to $G_{20}C_{klm}$ for a constant G_{20}, cf. (3.6). Using rescaling (3.9) with $\sigma_1 = \sigma_V = \sigma$ and $\sigma_U = 2\sigma$,

$$A_1 = \varepsilon^\sigma a_1, \qquad A_k = \varepsilon^{2\sigma}a_k, \qquad B_k = \varepsilon^\sigma b_k, \tag{5.5}$$

we derive a leading order amplitude system whose only difference from (3.11) is in the nonlinear terms for the b_k's. Switching to $\tau = \varepsilon^\sigma t$, we obtain a leading order set of amplitude equations,

$$\begin{aligned} a_1' &= ra_1 + C_{111}F_{20}a_1^2 + F_{11}a_1\sum_{m\geq 1}C_{11m}b_m \\ &\quad + F_{02}\sum_{l,m\geq 1}C_{1lm}b_lb_m + \mathcal{O}(\varepsilon^\sigma), \\ \varepsilon^\sigma a_k' &= \lambda_k a_k + C_{k11}F_{20}a_1^2 + F_{11}a_1\sum_{m\geq 1}C_{k1m}b_m \\ &\quad + F_{02}\sum_{l,m\geq 1}C_{klm}b_lb_m + \mathcal{O}(\varepsilon^\sigma), \\ \varepsilon^{\sigma-1}b_1' &= -M_1b_1 + \beta a_1 + \varepsilon^{\sigma-1}H_{111}a_1^2 + \mathcal{O}(\varepsilon^\sigma), \\ \varepsilon^{\sigma-1}b_k' &= -M_kb_k + \varepsilon^{\sigma-1}H_{k11}a_1^2 + \mathcal{O}(\varepsilon^\sigma). \end{aligned} \tag{5.6}$$

Here again, a prime represents differentiation with respect to τ and C_{klm}, H_{klm} are reported in (3.6) and (5.4).

For $\sigma > 1$, we recover classical center manifold reduction results, as was the case with (3.11). The slaving relations are

$$b_1 = \frac{\beta a_1}{M_1}, \qquad b_k = 0, \qquad a_k = \frac{C_{111}H}{\lambda_k}a_1^2, \tag{5.7}$$

compare with (3.13). Substituting into the ODE for a_1 and recalling definition (3.13), we can write

$$a_1' = ra_1 + C_{111}Ha_1^2 + \mathcal{O}(\varepsilon^\sigma). \tag{5.8}$$

Note that, in line with theory, the newly introduced nonlinearity does not affect classical center manifold reduction. This, however, changes as $\sigma \downarrow 1$: in that limit, and similar to system (3.11), the b_k-equations in system (5.6) retain their evolutionary character.

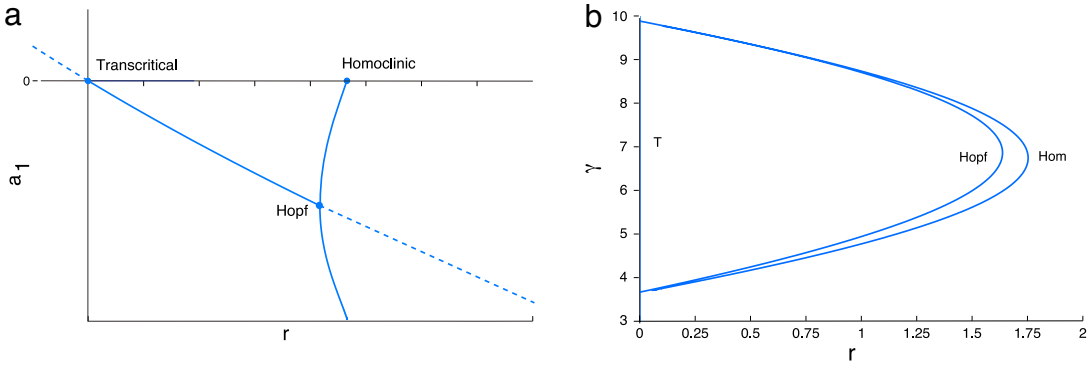

Fig. 5.1. Bifurcation figures of system (5.10), with parameters $\beta = -4, F_{20} = -2, F_{11} = 5, F_{02} = 12, A = 0.2$ and $B = 0.5$. (a) Steady state diagram in terms of the bifurcation parameter r and the first amplitude a_1; here, $\gamma = 5$. Solid (dashed) lines denote stable (unstable) equilibria. The points labeled 'T' and 'Hopf' indicate a transcritical (coincides with the vertical axis) and a Hopf bifurcation. The solid curves emerging from the Hopf bifurcation measure the minimum/maximum a_1-values of the bifurcating stable limit cycle. The limit cycle collides with the trivial steady state at 'Hom', yielding a homoclinic bifurcation. (b) A two-parameter continuation in (r, γ) of these three bifurcations; the transcritical one occurs at $r = 0$.

The system of ODEs governing the behavior of (5.2) in the regime $\lambda_1 = \mathcal{O}(\varepsilon)$ is, up to $\mathcal{O}(\varepsilon)$ corrections,

$$\begin{cases} a_1' = ra_1 + C_{111}F_{20}a_1^2 + F_{11}a_1 \sum_{n\geq 1} C_{1n1}b_n \\ \qquad + \sum_{m,n\geq 1} C_{mn1}F_{02}b_m b_n, \\ b_1' = -M_1 b_1 + \beta a_1 + H_{111}a_1^2, \\ b_k' = -M_k b_k + H_{k11}a_1^2, \quad \text{for } k \geq 2. \end{cases} \tag{5.9}$$

Asymptotically many b_k-modes interact now nonlinearly with the a_1-mode *at leading order*. Again, a rigorous proof of the validity of our asymptotic method is necessary, but not part of this paper.

Note that system (5.9) resembles but is not identical to the one corresponding to (1.1). The readily apparent differences between the two systems — linear coupling in (5.9) versus more quadratic terms in the other — are circumstantial and due to our working with (3.1), instead of with the eigenbasis as in [7]. A more appreciable difference concerns their coefficients, as the analogue of (3.6) in [7] involves two sets of eigenfunctions and is less transparent; recall Remark 4.2. Therefore, their corresponding flows may be widely different despite sharing the same functional form, see [22,16].

In the exploratory spirit of this paper, we choose not to study (5.9) in full generality but restrict ourselves, once again, to a transparent and highly illustrative special case.

5.2. Example: revisiting our reaction–diffusion system

We work with $\mathcal{L} = \Delta$, $\Omega = (0, 1)$ and homogeneous Dirichlet BCs, as in Section 2.2; the eigenfunctions are still given by the simple formulas (2.16). To reach a middle ground between the two-dimensional (4.2) and the infinite-dimensional (5.9), we choose

$$G_{20}(x) = \frac{2\sqrt{2}}{3}A\,\sin(\pi x) + \sqrt{2}B\sin(2\pi x),$$
$$\text{with } A, B \in \mathbb{R} \text{ free parameters.}$$

With this choice,

$$H_{111} = A, \qquad H_{112} = B, \qquad H_{113} = -\frac{1}{3}A,$$
$$H_{114} = -\frac{1}{2}B \quad \text{and} \quad H_{11k} = 0, \quad \text{for all } k \geq 5,$$

so that the ODEs for b_k, with $k \geq 5$, only contain higher order nonlinearities: at leading order, $\dot{b}_k = -M_k b_k$. From this we conclude that all b_k with $k \geq 5$ approach exponentially an $\mathcal{O}(\varepsilon)$ value. Thus, we obtain an explicit, exponentially attracting, 5-dimensional extended center manifold constraining b_k to $\mathcal{O}(\varepsilon)$ values, for $k \geq 5$, and with flow given by

$$\begin{cases} a_1' = ra_1 + C_{111}F_{20}a_1^2 + F_{11}\sum_{l\geq 1} C_{1l1}a_1 b_l + F_{02}\sum_{k,l\geq 1} C_{kl1}b_k b_l, \\ b_1' = -M_1 b_1 + \beta a_1 + A a_1^2, \\ b_2' = -M_2 b_2 + B a_1^2, \\ b_3' = -M_3 b_3 - \frac{1}{3}A a_1^2, \\ b_4' = -M_4 b_4 - \frac{1}{2}B a_1^2. \end{cases} \tag{5.10}$$

The differential equations for a_1, b_1, b_2, b_3 and b_4 characterize the behavior of the amplitudes in the direction of the modes linking to λ_1, μ_1, μ_2, μ_3 and μ_4. Note how the addition of a special, inhomogeneous, $\mathcal{O}(1)$ nonlinearity has yielded a 5-dimensional system as our extended center manifold reduction. We study this below using the ODE continuation toolbox MatCont, discussing two distinct parameter sets in some detail to illustrate behavioral diversity in it.

First, we fix $\beta = -4$, $\gamma = 5$, $F_{20} = -2$, $F_{11} = 5$ and $F_{02} = 12$ as in Figs. 4.1 and 4.2. Note that these figures concern system (1.3), which only has an $\mathcal{O}(\varepsilon)$, spatially homogeneous nonlinearity. Also note that $\gamma < \gamma_T = \pi^2$, so that the small spectrum is stable. We also fix $A = 0.2$ and $B = 0.5$, leaving r to vary. Fig. 5.1(a) provides a bifurcation diagram of the destabilization of the trivial steady state $(a_1, b_1, b_2, b_3, b_4) = (0, 0, 0, 0, 0)$ of (5.10). We track, as r increases, the branches bifurcating from zero using the first amplitude, a_1, as representative. In this way, we recover qualitatively the destabilization mechanism from Sections 2 and 4 (small, spatially homogeneous nonlinearity for V). Specifically, as r becomes positive, the trivial and nontrivial steady states exchange stability (transcritical). Tracking the nontrivial steady state for $r > 0$, we encounter a supercritical Hopf bifurcation at $r \approx 1.04$; of the stable limit cycle bifurcating from this point, we have drawn the minimum and maximum values of a_1. This limit cycle branch exists up to $r \approx 1.17$, where it becomes an orbit homoclinic to the trivial steady state. For larger r-values, we have found no other attractor. Note that this scenario corresponds precisely (albeit qualitatively) with our results in Sections 4.1 and 4.2.

Fig. 5.1(b) shows the continuation of these three bifurcations in two parameters: r and γ. This figure supports Conjecture 4.2 in the present case. If one increases r, starting from a negative value, then one first encounters a transcritical and then a supercritical Hopf bifurcation, which in turn is followed by a homoclinic bifurcation. Beyond this homoclinic bifurcation, orbits grow unboundedly and there seem to be no other attractors. At $(r, \gamma) = (0, \pi^2)$, there exists a transcritical Bogdanov–Takens point, see [18] for its

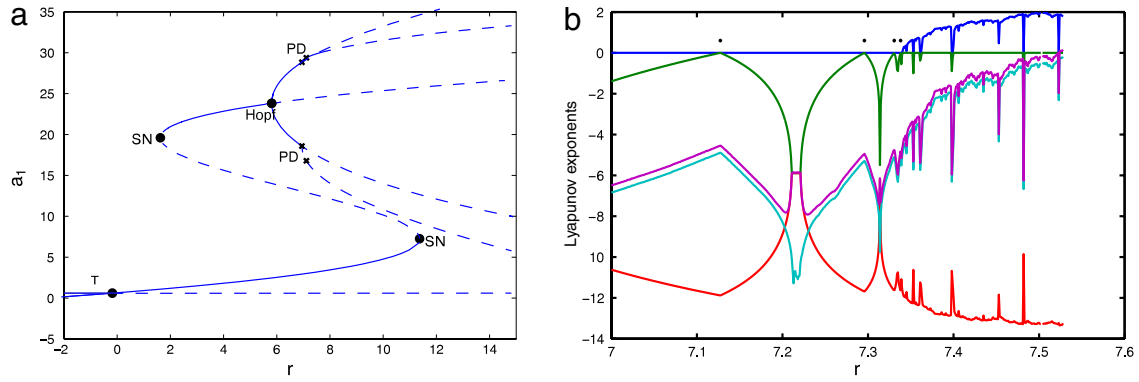

Fig. 5.2. (a) A bifurcation diagram corresponding to system (5.10). The parameter set is $\beta = -2.2$, $\gamma = 6$, $F_{20} = -0.6$, $F_{11} = 3$, $F_{02} = -3$, $A = 0.2$ and $B = 0.5$; r is varied. The nontrivial equilibrium first undergoes a transcritical bifurcation (T), then loses stability through a saddle–node bifurcation (SN), and becomes stable again through another saddle–node. After that, a supercritical Hopf bifurcation occurs (Hopf). We have plotted the maximum and minimum values of the stable limit cycles that arise. These undergo period-doubling bifurcations (PD), of which we marked two with an 'x'. (b) The five Lyapunov exponents corresponding to the chaotic orbit, shown with five different colors, varying with r. At $r \approx 7.34$, the first Lyapunov exponent becomes positive. At $r \approx 7.53$, the chaotic orbit collides with a saddle steady state, after which the chaotic orbit no longer exists. The black dots mark the r-values at which period-doubling bifurcations occur. (For interpretation of the references to color in this figure legend, the reader is referred to the web version of this article.)

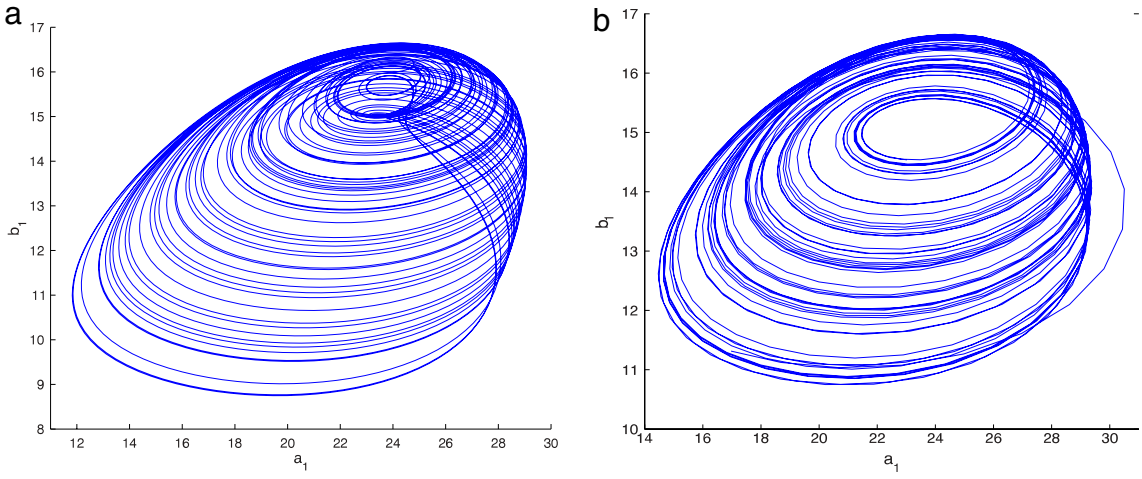

Fig. 5.3. Two similar chaotic attractors obtained by simulating the ODE (5.10) (left) and the PDE (5.2) (right), with $\beta = -2.2$, $\gamma = 6$, $F_{20} = -0.6$, $F_{11} = 3$, $F_{02} = -3$, $A = 0.2$ and $B = 0.5$. (a) $r = 7.49$. (b) $r = 7.7$, $\varepsilon = 0.01$ and $G_{20}(x) = \frac{2}{3}\sqrt{2}A\sin(\pi x) + \sqrt{2}B\sin(2\pi x)$. The operator is $\mathcal{L} = \Delta$ on the 1-dimensional domain $(0, 1)$ and with homogeneous Dirichlet boundary conditions.

unfolding. For negative values of r the bifurcation diagram is more subtle but we choose not to focus on that because this does not correspond to our analytical work.

For the parameter values reported above, we have seen no significant qualitative differences in the behavior of the reduced system (5.10) and of the original PDE system (1.3). This changes drastically if we retain $A = 0.2$ and $B = 0.5$ but switch to, for instance, $\beta = -2.2$, $\gamma = 6$, $F_{20} = -0.6$, $F_{11} = 3$ and $F_{02} = -3$. Using r as a bifurcation parameter, we observe that the transcritical bifurcation at $r = 0$ persists, see Fig. 5.2(a). Tracing the nontrivial steady state stabilized at $r = 0$, we see that it first encounters two saddle–node points at $r \approx 11.55$ and $r \approx 1.80$, before a Hopf bifurcation at $r \approx 5.99$ occurs. This Hopf bifurcation is supercritical, and again we have plotted the minimum and maximum of the limit cycle that arises there. Since this stable limit cycle exists for r-values where the nontrivial steady state is stable, there is bistability of both a steady state and a periodic solution. Contrary to the Hopf bifurcation in Fig. 5.1(a), the limit cycle here undergoes several period-doubling bifurcations and becomes chaotic, before terminating again in a homoclinic orbit for larger r-values ($r \approx 30$).

In Fig. 5.2(b), we have plotted all five Lyapunov exponents corresponding to the chaotic orbit from $r = 7$ onwards. At $r = 7.34$, the first Lyapunov exponent becomes positive, indicating chaos. Increasing r even further, the chaotic orbit persists and its magnitude grows, until it collides with a saddle steady state at $r = 7.53$. For larger values of r, all orbits escape to infinity. See Fig. 5.3(a), where the chaotic orbit itself is plotted for $r = 7.49$. In a simulation of the full PDE (1.3) with the same parameter values, we recover the same period-doubling scenario leading to chaos as in (1.1). However, at $r = 7.49$ the PDE is still in the '*double period-regime*', whereas the ODE reduction already shows a chaotic orbit. This can be understood by the fact that our approach only yields leading order accuracy and $\varepsilon = 0.01$. In principle, the incorporation of higher order terms is expected to improve the correspondence between the reduced and the full system, especially through the slaving relations for a_k with $k \geq 2$. Note that $a_1 \sim 15$–30 in the chaotic regime, thus $A_1 = \varepsilon a_1 \sim 0.15$–$0.30$, see (5.5) with $\sigma = 1$; this is already near the boundary for which one would expect an asymptotic method to work.

Remark 5.1. For parameters in a regime where the Hopf bifurcation is subcritical and with β small enough, we observe behavior similar to Fig. 5.1(b). In that case, the periodic orbit originating at the Hopf bifurcation exists for $r < r_H$, but it again accumulates onto a homoclinic orbit. The branch of homoclinic bifurcations in (r, γ)-space is now bounded by the transcritical branch to its left and the Hopf branch to its right.

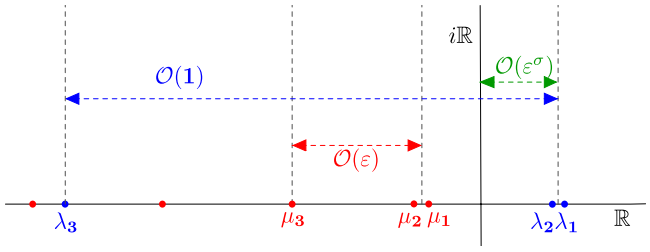

Fig. 6.1. Schematic depiction of a codimension 2 bifurcation where λ_1 and λ_2 pass through the origin, while all other eigenvalues remain in the stable half-plane.

6. Codimension 2 bifurcations

As explained in the Introduction, it was analyzed in [6] that the organizing center of chaos in the phytoplankton-nutrient model (1.1) corresponds to a codimension 2 bifurcation — a point where two eigenvalues cross the imaginary axis simultaneously. In this section, we investigate the type of phenomena that such points can give rise to, within the context of our model problem (1.3). In the specific case of (1.1), the small spectrum remains contained in the negative semi-axis for all parameter values [7]. We therefore also focus on the case where (also) the second eigenvalue crossing the origin is '*large*'. It is neither our intention nor within the scope of this paper to offer a complete treatment of all possible transcritical codimension 2 bifurcations in system (1.3). We are primarily interested, instead, in giving an indication of the variety of low-dimensional dynamics exhibited by (1.3) and related models in a codimension 2 setting, which are not captured by classical center manifold reduction.

We present our work below in the general setting of a multidimensional bounded domain $\Omega \subset \mathbb{R}^n$. In Section 6.1, we construct and treat an abstract codimension 2 situation, where the two leading eigenvalues λ_1 and λ_2 of $\mathcal{DT}$ cross zero simultaneously in a two-component system (i.e., with scalar U and V). See Proposition 2.1 and Fig. 6.1. We then reduce the PDE system to a 4-dimensional ODE one. Subsequently, in Section 6.2, we consider another type of codimension 2 bifurcation obtained by adding an extra component to system (1.3). We find there, in turn, that the flow on the extended center manifold is 3-dimensional, illustrating our results further by means of our exemplary reaction–diffusion example with an additional component.

6.1. Coincidence of the two largest eigenvalues

We first consider the case in which λ_1 and λ_2 cross through the imaginary axis simultaneously, as is depicted in Fig. 6.1. Recalling the characterization of eigenvalues in Proposition 2.1, we conclude that the two largest eigenvalues of $\mathcal{L}$ — recall the associated spectral problem (2.3) — are necessarily equal, $\nu_1 = \nu_2$. We show that, in this case, our PDE system (1.3) is reducible to a 4-dimensional ODE system close to the bifurcation, and we examine the rich dynamics of that reduced system.

Note for definiteness that, in our exemplary choice $\mathcal{L} = \Delta$ with homogeneous Dirichlet BCs on a bounded domain $\Omega \in \mathbb{R}^n$, the first eigenvalues cannot collide [9,13]. However, there exist combinations of operators, spatial domains and BCs for which assumptions A1–A3 are satisfied and $\nu_1 = \nu_2$ holds. One such example is $\mathcal{L} = -\Delta^2$ considered on an annulus and with homogeneous BCs for the zeroth and second order derivatives, see [9] for details. Following ideas from that work, we parameterize by a scalar parameter κ a 1-dimensional, continuous family of bounded domains $\{\Omega_\kappa\}_\kappa$, with piecewise continuous boundaries. The eigenvalues ν_k corresponding to linear differential operator $\mathcal{L}$ are thus parameterized by κ too, so we write $\{\nu_k(\kappa)\}_k$ for the spectrum of this operator on Ω_κ. To set us up for our analysis, we next assume the existence of a κ^* for which

$$\cdots < \nu_3(\kappa^*) < \nu_2(\kappa^*) = \nu_1(\kappa^*),$$

and we further assume, for ν_1 and ν_2, asymptotic expansions in powers of κ up to first-order:

$$\nu_i(\kappa) = \nu_1(\kappa^*) + (\kappa - \kappa^*)\nu_{i,1}(\kappa^*) + \mathcal{O}(|\kappa - \kappa^*|^2),$$
$$\text{for } i = 1, 2 \text{ and with } \nu_{1,1}(\kappa^*) \neq \nu_{2,1}(\kappa^*).$$

Finally, to avoid introducing generalized eigenfunctions, we further assume that the eigenspaces corresponding to these two eigenvalues do not coincide, as $\kappa \to \kappa^*$ — this is also the case for $-\Delta^2$ considered in [9].

At $\kappa = \kappa^*$, the equality $\nu_1 = \nu_2$ automatically yields $\lambda_1 = \lambda_2$ and $\mu_1 = \mu_2$ for the eigenvalues of $\mathcal{DT}$, see (2.7)–(2.8). Note that the equality $\mu_1 = \mu_2$ is an inadvertent consequence of modeling the evolution of U and V by the same operator $\mathcal{L}$. We additionally assume the small spectrum to remain '*harmless*' (negative) and set for our analysis

$$\kappa = \kappa^* + s\varepsilon^\sigma, \quad \text{with } s \in \mathbb{R} \text{ and } \sigma > 0.$$

The asymptotic expansions for ν_1 and ν_2 allow us to write, then,

$$\nu_1(\kappa) = \nu_1(\kappa^*) + s\varepsilon^\theta \nu_{1,1}(\kappa^*) + \mathcal{O}(\varepsilon^{2\theta}),$$
$$\nu_2(\kappa) = \nu_1(\kappa^*) + s\varepsilon^\theta \nu_{2,1}(\kappa^*) + \mathcal{O}(\varepsilon^{2\theta}).$$

As usual, we rescale α according to

$$\alpha = r\varepsilon^\sigma - \nu_1(\kappa^*) \quad \text{and also demand that } \gamma < \gamma_T,$$

thus positioning λ_1 and λ_2 at an $\mathcal{O}(\varepsilon^\sigma)$ distance inside the right half of the complex plain. Here again, r is the bifurcation parameter; the eigenvalues are, to leading order,

$$\begin{aligned} \lambda_1(\kappa) &= (r + s\nu_{1,1}(\kappa^*))\varepsilon^\sigma = \varepsilon^\sigma L_1, \\ \lambda_2(\kappa) &= (r + s\nu_{2,1}(\kappa^*))\varepsilon^\sigma = \varepsilon^\sigma L_2. \end{aligned} \tag{6.1}$$

As before, we set $\mu_k = -\varepsilon M_k$ and consider (L_1, L_2) as new and independent bifurcation parameters. Note that varying them is equivalent to varying (r, s), since $\nu_{1,1}(\kappa^*) \neq \nu_{2,1}(\kappa^*)$ by assumption. Further, we assume the setting of Section 4, where the nonlinearity co-driving V is weak. Returning to the basic system (1.3) and substituting amplitude expansion (3.2), then, we again obtain system (3.7) but with two weakly unstable A_k-modes. This is not surprising, as the A_k-modes link directly to the two destabilizing eigenvalues λ_1 and λ_2; all other modes remain stable. We thus rescale the amplitudes accordingly,

$$A_1 = \varepsilon^\sigma a_1, \qquad A_2 = \varepsilon^\sigma a_2, \qquad A_k = \varepsilon^{2\sigma} a_k \quad \text{for } k \geq 3 \quad \text{and}$$
$$B_k = \varepsilon^\sigma b_k \quad \text{for } k \geq 1, \text{ with } \sigma > 0.$$

The amplitude system becomes,

$$\begin{aligned} a_i' &= L_i a_i + F_{20}(C_{i11}a_1^2 + 2C_{i21}a_1a_2 + C_{i22}a_2^2) \\ &\quad + F_{11}\left(a_1 \sum_{m\geq 1} C_{i1m}b_m + a_2 \sum_{m\geq 1} C_{i2m}b_m\right) \\ &\quad + F_{02} \sum_{l,m\geq 1} C_{ilm}b_l b_m, \quad \text{for } i = 1, 2, \\ \varepsilon^\sigma a_k' &= \lambda_k a_k + F_{20}\left(C_{k11}a_1^2 + 2C_{k12}a_1a_2 + C_{k22}a_2^2\right) \\ &\quad + F_{11}\left(a_1 \sum_{m\geq 1} C_{k1m}b_m + a_2 \sum_{m\geq 1} C_{k2m}b_m\right) \\ &\quad + F_{02} \sum_{l,m\geq 1} C_{klm}b_l b_m, \quad \text{for } k \geq 3, \\ \varepsilon^\sigma b_i' &= -\varepsilon M_i b_i + \varepsilon\beta a_i, \quad \text{for } i = 1, 2, \\ \varepsilon^\sigma b_k' &= -\varepsilon M_k b_k, \quad \text{for } k \geq 3, \end{aligned} \tag{6.2}$$

to leading order and expressed in $\tau = \varepsilon t$. Again, a critical transition occurs when $\sigma = 1$, see (3.11), in which regime the spectral gap condition is violated.

We first consider the case $\sigma > 1$, in which the spectral gap is of sufficient width. The leading order slaving relations are, then,

$$b_1 = \frac{\beta a_1}{M_1}, \qquad b_2 = \frac{\beta a_2}{M_2} \quad \text{and} \quad b_k = 0, \quad \text{for } k \geq 3. \tag{6.3}$$

The center manifold – in the classical sense, since $\sigma > 1$ – is 2-dimensional, with the flow on it given by

$$\begin{cases} a_1' = L_1 a_1 + C_{111} H_{11} a_1^2 + 2C_{121} H_{12} a_1 a_2 + C_{122} H_{22} a_2^2, \\ a_2' = L_2 a_2 + C_{211} H_{11} a_1^2 + 2C_{221} H_{12} a_1 a_2 + C_{222} H_{22} a_2^2. \end{cases} \tag{6.4}$$

Here, we have applied the slaving relations and defined the quantities

$$H_{ij} = F_{20} + \frac{F_{11}\beta}{2}\left(\frac{1}{M_i} + \frac{1}{M_j}\right) + \frac{F_{02}\beta^2}{M_i M_j}, \quad \text{for } i, j = 1, 2.$$

This is as expected, for a degenerate codimension 2 transcritical bifurcation of the present type. Moreover, $M_1 = M_2 + \mathcal{O}(\varepsilon^{\sigma-1})$, since $\nu_1 = \nu_2 + \mathcal{O}(\varepsilon^\sigma)$. Hence, $H_{11} = H_{12} = H_{22} = H$ at leading order, cf. (3.13), and (6.4) simplifies to

$$\begin{cases} a_1' = L_1 a_1 + H\left(C_{111} a_1^2 + 2C_{112} a_1 a_2 + C_{122} a_2^2\right), \\ a_2' = L_2 a_2 + H\left(C_{112} a_1^2 + 2C_{122} a_1 a_2 + C_{222} a_2^2\right). \end{cases} \tag{6.5}$$

Note that the validity of center manifold reduction can, in principle, be rigorously established by classical methods [1–3]. The trivial state $(U, V) = (0, 0)$, represented by $(a_1, b_1) = (0, 0)$, remains a steady state with eigenvalues $\Lambda_1 = L_1$ and $\Lambda_2 = L_2$. Since steady states now correspond to intersections of two conic sections, there are up to three more steady states (a_1^*, a_2^*) with Jacobian matrix

$$\begin{aligned} &J(a_1^*, a_2^*) \\ &= \begin{pmatrix} L_1 + 2H\left(C_{111}a_1^* + C_{112}a_2^*\right) & 2H\left(C_{112}a_1^* + C_{122}a_2^*\right) \\ 2H\left(C_{112}a_1^* + C_{122}a_2^*\right) & L_2 + 2H\left(C_{122}a_1^* + C_{222}a_2^*\right) \end{pmatrix} \\ &= \begin{pmatrix} J_{11} & J_{12} \\ J_{12} & J_{22} \end{pmatrix}. \end{aligned}$$

Note that the off-diagonal terms are equal; the eigenvalues $\Lambda_\pm$ of matrices of this form are

$$\Lambda_\pm = \frac{J_{11} + J_{22} \pm \sqrt{(J_{11} - J_{22})^2 + 4J_{12}^2}}{2},$$

and they are necessarily real. Hence, none of the steady states can undergo oscillatory destabilization. The two eigenvalues can, however, change signs when $J_{11}J_{22} = J_{12}^2$, and a fixed point may gain or lose stability.

Next, we analyze the regime $\sigma = 1$ for system (6.2). Here again, the b_k-amplitudes are no longer slaved but evolve in the same timescale as a_1 and a_2. Up to $\mathcal{O}(\varepsilon)$ corrections,

$$\begin{aligned} a_i' &= L_i a_i + F_{20}\left(C_{i11}a_1^2 + 2C_{i21}a_1a_2 + C_{i22}a_2^2\right) \\ &\quad + F_{11}\left(a_1 \sum_{m\geq 1} C_{i1m} b_m + a_2 \sum_{m\geq 1} C_{i2m} b_m\right) \\ &\quad + F_{02} \sum_{l,m\geq 1} C_{ilm} b_l b_m, \quad \text{for } i = 1, 2, \\ b_i' &= -M_i b_i + \beta a_i, \quad \text{for } i = 1, 2, \\ b_k' &= -M_k b_k \quad \text{for } k \geq 3. \end{aligned} \tag{6.6}$$

System (6.6) contains two quadratically nonlinear ODEs and infinitely many linear ones. Similar to Section 4.1, the b_k-modes for $k \geq 3$ decouple, at leading order, and are slaved to $\mathcal{O}(\varepsilon)$ values. We formally conclude that, in this extended region and codimension 2 setting, the small amplitude flow of the PDE system (1.3) is attracted to a 4-dimensional invariant manifold, the flow on which is approximately described by

$$\begin{aligned} a_i' &= L_i a_i + F_{20}\left(C_{i11}a_1^2 + 2C_{i21}a_1a_2 + C_{i22}a_2^2\right) \\ &\quad + F_{11}a_1\left(C_{i11}b_1 + C_{i12}b_2\right) \\ &\quad + F_{11}a_2\left(C_{i21}b_1 + C_{i22}b_2\right) \\ &\quad + F_{02}\left(C_{i11}b_1^2 + 2C_{i12}b_1b_2 + C_{i22}b_2^2\right), \quad \text{for } i = 1, 2. \\ b_i' &= -M_i b_i + \beta a_i, \end{aligned} \tag{6.7}$$

The validity of this reduction is not proved in this study. We refrain from delving into the characteristics of this flow, as the sheer number of parameters ensures the existence of rich dynamics. We do note, however, that the corresponding equilibria will naturally undergo Hopf bifurcations. Thus, also in this, codimension 2 case, transcritical bifurcations may generally be followed by Hopf bifurcations within an $\mathcal{O}(\varepsilon)$ neighborhood.

6.2. A three-component system

We consider an extended version of system (1.3), namely the 3-component model (1.5) from the Introduction. The operator $\mathcal{L}$, spatial domain Ω and BCs satisfy assumptions A1–A3. The constants $\alpha_1, \alpha_2, \beta_1, \beta_2, \rho_2$ and γ are all real, and the nonlinearities $F_1(U_1, U_2, V)$, $F_2(U_1, U_2, V)$ and $G(U_1, U_2, V)$ are smooth functions of their arguments. Moreover, we have introduced '*diffusion*' coefficients $D_1, D_2 > 0$, both of which are $\mathcal{O}(1)$ with respect to ε; this is natural in reaction–diffusion 3-component models, since $D_1 \neq D_2$ in general. More importantly, we have now the V-component feeding into the U_2-equation also linearly, if weakly; cf. the term $\varepsilon\rho_2 V$ in the system. No such mechanism exists for U_1, as was also the case in system (1.3). The rationale behind this *weak* extension of the core system (1.3) is its becoming significant in the *leading order* extended center manifold reduction (ECMR) we derive below. In that, it highlights how different unfoldings of the primary bifurcation may excite different dynamic modes in the ECMR regime.

By construction, the background state $(U_1, U_2, V) \equiv (0, 0, 0)$ has 3 distinct sets of eigenvalues. Assuming that both $\alpha_2 + D_2\nu_k$ and $\gamma + \nu_k$ are $\mathcal{O}(1)$ and bounded away from zero, it follows quite straightforwardly that, for $k \geq 1$,

$$\begin{aligned} \lambda_{1,k} &= \alpha_1 + D_1\nu_k, \\ \lambda_{2,k} &= \alpha_2 + D_2\nu_k + \mathcal{O}(\varepsilon^2), \\ \mu_k &= \varepsilon(\gamma + \nu_k) + \mathcal{O}(\varepsilon^2) = -\varepsilon M_k + \mathcal{O}(\varepsilon^2), \end{aligned} \tag{6.8}$$

with ν_k the eigenvalue associated with $\mathcal{L}$ – see Proposition 2.1 and Fig. 1.1. Here, $\lambda_{1,k}$ is associated with the PDE for U_1 and boundary conditions, and $\{\lambda_{2,k}\}_{k\geq 1}$ is the spectrum associated with U_2 and the boundary conditions. Thus, the 'new' term $\varepsilon\rho_2 V$ only has an $\mathcal{O}(\varepsilon^2)$ effect on both $\lambda_{2,k}$ and μ_k. In the bifurcational case where we set $\alpha_2 + D_2\nu_1 = r_2\varepsilon^\sigma$, with $\sigma \geq 1$ and $r_2 = \mathcal{O}(1)$, the effect of ρ_2 through $\varepsilon\rho_2 V$ is larger – $\mathcal{O}(\varepsilon^{2-\sigma})$. Even though $\gamma + \nu_k \neq 0$ is still $\mathcal{O}(1)$, ρ_2 also impacts μ_1. In fact, in the critical case $\sigma = 1$, the eigenvalues $\lambda_{2,1}$ and μ_1 are both $\mathcal{O}(\varepsilon)$ and they are the solutions L of the equation

$$L^2 + \varepsilon L(M_1 - r_2) - \varepsilon^2(r_2 M_1 + \beta_2\rho_2) = 0. \tag{6.9}$$

However, except for some notational inconveniences, this feature has no effect on our method.

Our aim is to study the codimension 2 transcritical bifurcation in which the 'large' primary eigenvalues $\lambda_{1,1}$ and $\lambda_{2,1}$ cross zero simultaneously. Before that, we first understand the codimension 1 case, where only $\lambda_{1,1}$ is $\mathcal{O}(\varepsilon^\sigma)$ close to zero and $\lambda_{2,1}$ far behind it; here, $\sigma \geq 1$ as in Section 4. To set up our analysis, we assume that $\alpha_2 + D_2\nu_1 < 0$ and $\gamma + \nu_1 < 0$ are $\mathcal{O}(1)$. Mimicking our approach

in Section 3, cf. (3.2), we introduce the amplitudes $A_{1,k}(t)$, $A_{2,k}(t)$ and $B_k(t)$ through

$$\begin{pmatrix} U_1(x,t) \\ U_2(x,t) \\ V(x,t) \end{pmatrix} = \sum_{k\geq 1} \phi_k(x) \begin{pmatrix} A_{1,k}(t) \\ A_{2,k}(t) \\ B_k(t) \end{pmatrix}. \tag{6.10}$$

Here the (rescaled) amplitudes $A_{1,k}$, $A_{2,k}$ and B_k link directly to the eigenvalues $\lambda_{1,k}$, $\lambda_{2,k}$ and μ_k. The new coupling term $\varepsilon\rho_2 V$ suggests a rescaling differing in the particulars from that of Section 3,

$$\begin{aligned} &\lambda_{1,1} = r_1\varepsilon^\sigma, \qquad A_{1,1} = \varepsilon^\sigma a_{1,1}, \qquad A_{1,k} = \varepsilon^{2\sigma} a_{1,k}, \\ &A_{2,\ell} = \varepsilon^{1+\sigma} a_{2,\ell} \quad \text{and} \quad B_\ell = \varepsilon^\sigma b_\ell, \end{aligned} \tag{6.11}$$

for $k \geq 2$ and $l \geq 1$. We also write $M_k = -(\gamma + \nu_k)$, as for the two-components system (1.3), and expand the nonlinearities restricting to quadratic terms, cf. (3.4). For $i = 1, 2$, then,

$$\begin{aligned} F_i(U,V) &= F_{i,200}U_1^2 + F_{i,110}U_1U_2 + F_{i,101}U_1V \\ &\quad + F_{i,020}U_2^2 + F_{i,011}U_2V + F_{i,002}V^2, \\ G(U,V) &= G_{200}U_1^2 + G_{110}U_1U_2 + G_{101}U_1V \\ &\quad + G_{020}U_2^2 + G_{011}U_2V + G_{002}V^2. \end{aligned} \tag{6.12}$$

For $\sigma > 1$, classical center manifold reduction is possible with the equivalent of (3.14) being

$$a'_{1,1} = r_1 a_{1,1} + C_{111}H_1 a_{1,1}^2 + \mathcal{O}(\varepsilon); \tag{6.13}$$

here, the time derivative is taken with respect to $\tau = \varepsilon^\sigma t$ and

$$H_1 = F_{1,200} + \frac{F_{1,101}\beta_1}{M_1} + \frac{F_{1,002}\beta_1^2}{M_1^2}. \tag{6.14}$$

This ODE is coupled to the slaving relations,

$$\begin{aligned} a_{1,k} &= -\frac{1}{\lambda_{1,k}}\left[C_{11k}H_1 a_{1,1}^2\right] + \mathcal{O}(\varepsilon), \\ a_{2,1} &= -\frac{\rho_2\beta_1}{M_1\lambda_{2,1}} a_{1,1} + \mathcal{O}(\varepsilon^{\sigma-1}), \\ a_{2,k} &= 0 + \mathcal{O}(\varepsilon^{\sigma-1}), \\ b_1 &= \frac{\beta_1}{M_1} a_{1,1} + \mathcal{O}(\varepsilon^{\sigma-1}, \varepsilon^2), \\ b_k &= 0 + \mathcal{O}(\varepsilon^{\sigma-1}), \end{aligned} \tag{6.15}$$

where $k \geq 2$. All $a_{2,k}$-modes except for the first one behave, then, as additional b_k-modes for $\sigma > 1$. The eigenvalues $\lambda_{2,k}$, $k \geq 2$ induce the same kind of behavior as the μ_k induce. This changes beyond center manifold reduction, as $\sigma \downarrow 1$. In that regime, the $a_{2,k}$-modes ($k \geq 2$) remain slaved – now to both $a_{1,1}$ and b_1 – but neither $a_{2,k}$ nor b_k with $k \geq 2$ are higher order anymore; we find that $b'_k = -M_k b_k$ at leading order ($k \geq 2$), similar to (4.1). We therefore have $b_k = \mathcal{O}(\varepsilon)$ for those k-values and may rewrite the three-component system (1.5) as a 2-dimensional system of amplitude equations resembling (4.2),

$$\begin{cases} a'_{1,1} = r_1 a_{1,1} \\ \quad + C_{111}\left(F_{1,200}a_{1,1}^2 + F_{1,101}a_{1,1}b_1 + F_{1,002}b_1^2\right) + \mathcal{O}(\varepsilon), \\ b'_1 = -M_1 b_1 + \beta_1 a_{1,1} + \mathcal{O}(\varepsilon). \end{cases} \tag{6.16}$$

The evolution of the slaved modes is dictated by this system and the slaving relations,

$$\begin{aligned} a_{1,k} &= -\frac{1}{\lambda_{1,k}}\left[C_{11k}\left(F_{1,200}a_{1,1}^2\right.\right. \\ &\quad \left.\left. + F_{1,101}a_{1,1}b_1 + F_{1,002}b_1^2\right)\right] + \mathcal{O}(\varepsilon), \quad \text{for } k \geq 2, \end{aligned}$$

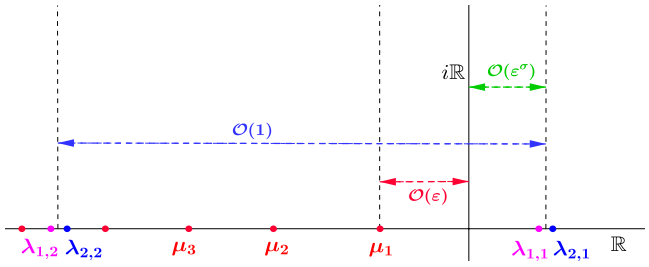

Fig. 6.2. Schematic representation of the eigenvalues determining the stability of $(U_1, U_2, V) = (0, 0, 0)$ in system (1.5) and in the codimension 2 setting (6.19). All eigenvalues are negative except for the primary ones, $\lambda_{1,1}$ and $\lambda_{2,1}$,which are positive and $\mathcal{O}(\varepsilon^\sigma)$. All three eigenvalue sets are unbounded below.

$$\begin{aligned} a_{2,1} &= -\frac{1}{\lambda_{2,1}}\left[C_{111}\left(F_{2,200}a_{1,1}^2\right.\right. \\ &\quad \left.\left. + F_{2,101}a_{1,1}b_1 + F_{2,002}b_1^2\right) + \rho_2 b_1\right] + \mathcal{O}(\varepsilon), \\ a_{2,k} &= -\frac{1}{\lambda_{2,k}}\left[C_{11k}\left(F_{2,200}a_{1,1}^2\right.\right. \\ &\quad \left.\left. + F_{2,101}a_{1,1}b_1 + F_{2,002}b_1^2\right)\right] + \mathcal{O}(\varepsilon), \quad \text{for } k \geq 2. \end{aligned}$$

Thus, we may conclude that the (codimension 1) transcritical bifurcation generates precisely the same behavior in the 3-component model (1.5) as in the 2-component one (1.3) up to and including the regime $\sigma = 1$ covered by extended center manifold reduction.

We now proceed to analyze the codimension 2 bifurcation. To facilitate our presentation, we introduce the quadratic polynomials (cf. (6.12))

$$\begin{aligned} \mathcal{F}_j(a,b,c) &= F_{j,200}a^2 + F_{j,110}ab + F_{j,101}ac \\ &\quad + F_{j,020}b^2 + F_{j,011}bc + F_{j,002}c^2, \quad j = 1, 2. \end{aligned} \tag{6.17}$$

Note that (6.13), for instance, can now be rewritten as

$$a'_{1,1} = r_1 a_{1,1} + C_{111}\,\mathcal{F}_1(a_{1,1}, 0, \beta_1 a_{1,1}/M_1) + \mathcal{O}(\varepsilon). \tag{6.18}$$

The polynomials $\mathcal{F}_j$ can be similarly introduced in (6.14), as well as in the slaving relations (6.15). To generate a codimension 2 bifurcation, we tune D_1, D_2, α_1, α_2 and introduce r_1, r_2 by

$$\begin{aligned} &\alpha_1 + D_1\nu_1 = \lambda_{1,1} = r_1\varepsilon^\sigma \quad \text{and} \\ &\alpha_2 + D_2\nu_1 = r_2\varepsilon^\sigma, \quad \text{with } \sigma \geq 1, \end{aligned} \tag{6.19}$$

cf. (6.8); the spectrum is depicted in Fig. 6.2. Note that $\alpha_2 + D_2\nu_1 \neq \lambda_{2,1}$; the equality only holds at leading order, due to the presence of $\varepsilon\rho_2 V$ in (1.5); cf. (6.8) again. We also set $M_k = -(\gamma + \nu_k)$ and assume M_1 to be $\mathcal{O}(1)$ and nonzero but not necessarily negative.

We skip the case $\sigma > 1$ (but see Remark 6.1) and proceed immediately to $\sigma = 1$. We rescale as

$$\begin{aligned} &A_{1,1} = \varepsilon^\sigma a_{1,1}, \qquad A_{1,k} = \varepsilon^{2\sigma} a_{1,k}, \qquad A_{2,1} = \varepsilon^\sigma a_{2,1}, \\ &A_{2,k} = \varepsilon^{\sigma+1} a_{2,k} \quad \text{and} \quad B_\ell = \varepsilon^\sigma b_\ell, \end{aligned} \tag{6.20}$$

for $k \geq 2$ and $\ell \geq 1$, see (6.10). The $a_{1,k}$- and $a_{2,k}$-modes remain slaved for all $k \geq 2$, while again $b_k = -M_k b_k$ at leading order; the situation is analogous to the two-component case, recall Section 4. Following the path we carved in that case, we restrict ourselves naturally to the exponentially attracting subspace $\{b_k = \mathcal{O}(\varepsilon)\}_{k\geq 2}$. Up to $\mathcal{O}(\varepsilon)$ corrections, then, the a priori infinite-dimensional flow reduces to a 3-dimensional one,

$$\begin{cases} a'_{1,1} = r_1 a_{1,1} + C_{111}\,\mathcal{F}_1(a_{1,1}, a_{2,1}, b_1), \\ a'_{2,1} = r_2 a_{2,1} + \rho_2 b_1 + C_{111}\,\mathcal{F}_2(a_{1,1}, a_{2,1}, b_1), \\ b'_1 = \beta_1 a_{1,1} + \beta_2 a_{2,1} + (\gamma + \nu_1) b_1. \end{cases} \tag{6.21}$$

It thus turns out that the three-component, codimension 2 equivalent of the two-component, codimension 1 (planar and quadratic)

extended center manifold reduction (6.16) is the 3-dimensional, quadratic system (6.21). In this paper, we study neither the dynamics generated by system (6.21) nor the bifurcational structure associated with it in any detail; we have done so for the planar flow generated by (6.16), recall Sections 4.1 and 4.2. We do, however, observe that the celebrated Lorenz system [10] belongs to the family of systems described by (6.21), as can be seen by setting

$$x(t) = b_1(\tau), \qquad y(t) = a_{2,1}(\tau), \qquad z(t) = a_{1,1}(\tau),$$

and choosing the $F_{j,klm}$-coefficients of $\mathcal{F}_j(z, y, x)$, see (6.17), so that

$$C_{111}\mathcal{F}_1(z, y, x) = xy \quad \text{and} \quad C_{111}\mathcal{F}_2(z, y, x) = -xz.$$

Then, (6.21) reduces to

$$\begin{cases} \dot{x} = (\gamma + \nu_1)x + \beta_2 y + \beta_1 z, \\ \dot{y} = \rho_2 x + r_2 y - xz, \\ \dot{z} = r_1 z + xy, \end{cases} \tag{6.22}$$

which is equivalent to the Lorenz system with parameters (σ, b, r), upon setting

$$(r_1, r_2, \beta_1, \beta_2, \gamma, \rho_2) = (-b, -1, 0, \sigma, -\sigma - \nu_1, r).$$

Note that, at first glance, setting both r_1 and r_2 negative suggests that $\lambda_{1,1}$ and $\lambda_{2,1}$ are stable. However, recall that we have set $\alpha_2 + D_2\nu_1 = r_2\varepsilon$, and the eigenvalues of the trivial state are not represented by (6.8) but rather as solutions of (6.9) instead. A direct check yields that $\lambda_{1,1}, \lambda_{2,1}, \mu_1$ indeed correspond directly to the eigenvalues of the unstable critical point $(0, 0, 0)$ of (6.22).

It is apparent in our approach, but we nevertheless underline it here, that there is a significant difference between our derivation of (6.21) and the derivation of the Lorenz model. In particular, the Lorenz model is a *truncation* of the full flow of the infinite-dimensional convective system considered in [10], which approximates neither quantitatively nor qualitatively the dynamics of that original model; see [11] and the Introduction. Instead, (6.21) describes the flow on a 3-dimensional manifold which *attracts by construction* the dynamics of small amplitude solutions – scaled as in (6.20) – of the singularly perturbed evolution equation (1.5). It is for this reason that (6.21) *does* approximate the full dynamics of (1.5) asymptotically: see Fig. 1.2, where the celebrated Lorenz butterfly is plainly visible. Note that the figure was produced by a direct simulation of the PDE system (1.5), with $\mathcal{L} = \Delta, \Omega = (0, 1)$, Dirichlet BCs – similar to Section 2.2 – and all parameters tuned to the standard chaotic parameter combination $(\sigma, b, r) = (10, 8/3, 28)$ in the Lorenz model. Indeed, for these parameter values – as in Fig. 1.2 – the solutions of (6.9) are $\lambda_{2,1} > 0$ and $\mu_1 < 0$. Moreover, it should be noted that we have also recovered the Lorenz attractor for systems (1.5) with nonlinearities that are more general than the exactly quadratic ones given in the caption of Fig. 1.2. Only the leading order quadratic approximations (6.12) need to be as described above, higher order nonlinearities do not have a leading order impact. For example, choosing $F_1(U_1, U_2, V) = 3\sqrt{2}\pi/16 \sin(U_2 V)$ as opposed to $F_1(U_1, U_2, V) = 3\sqrt{2}\pi/16 U_2 V$ which we have used now, works just as well.

Remark 6.1. The codimension 2 case with $\sigma > 1$ is, due to our rescaling, slightly different from what we expect. All modes are slaved to $a_{1,1}$ — related to the eigenvalue $\lambda_{1,1}$, see Fig. 6.2 —, even though this is a codimension 2 situation. This has to do with the fact that, for $\sigma > 1$, the magnitude of $A_{1,k}$ is scaled differently from $A_{2,k}$, see (6.20). We refrain from elaborating further in this paper.

7. Discussion

In this article, we have discussed the extension of center manifold reduction (CMR), a classical nonlinear method for dimension reduction. We have chosen, as our setting, the transcritical bifurcation destabilizing a trivial background state of a singularly perturbed, multi-component, evolutionary PDE model. CMR operates locally to the parameter regime where the destabilization occurs and as long as a certain spectral gap condition is satisfied. We have exemplified its extension to regions in parameter space where that condition is violated and termed our approach *extended* center manifold reduction (ECMR). Our approach was crafted in the context of a number of explicit and closely related model problems, see (1.3), (1.5) and (5.1). However, this work has been inspired by and builds on an earlier study of a very different model, namely the phytoplankton-nutrient model (1.1). Model (1.1) has the same basic structure as these model problems, which enables ECMR. This structure unsurprisingly concerns the *spectrum* determining the stability of the trivial background state and is drawn schematically in Figs. 1.1, 6.1 and 6.2. Specifically, ECMR hinges on the assumption that the spectrum in question partitions into families $\{\lambda_k\}_k$ and $\{\mu_k\}_k$ of '*large*' and '*small*' eigenvalues, respectively. It is thus expected to be applicable to the general class of systems given in (1.2), see also [8]. In this paper, and for any fixed k, λ_k and μ_k are $\mathcal{O}(1)$ and $\mathcal{O}(\varepsilon)$, respectively, for an asymptotically small parameter ε.

Our analysis treats situations where one or two of the large eigenvalues initiate a bifurcation by crossing through zero while all others remain stable. Linear theory suffices to pinpoint the codimension 1 or 2 surface (in parameter space) where the bifurcation occurs and, additionally, predicts the 'shape' of the bifurcating pattern. The nonlinear extension of center manifold reduction improves on linear theory by predicting the amplitude of that pattern, and tracking it along a larger parametric regime. This regime is restricted, nevertheless, in that the 'eventual fate' of the pattern lies even further beyond. The underlying reason is that CMR validity is relying on the existence of a spectral gap of sufficient width; simply put, the critical (i.e. bifurcating) eigenvalues λ_j must be sufficiently closer to the imaginary axis than the largest stable eigenvalue μ_1. In our setting, this condition reads $|\lambda_j| = \mathcal{O}(\varepsilon^\sigma) \ll \mathcal{O}(\varepsilon) = |\mu_1|$ so $\sigma > 1$. ECMR, in turn, improves this state of affairs by operating in the 'gapless' limit $\sigma = 1$. A priori, one would expect a large number of μ_k-modes to be excited in that case, since μ_k scale with ε. In the singularly perturbed setting considered here, however, it turns out that only the μ_1-mode contributes appreciably to the dynamics. The classical, 1-dimensional CMR describing a codimension 1 transcritical bifurcation must hence be extended to a merely 2-dimensional extended center manifold. The resulting reduced dynamics attract small initial conditions at an exponential rate and well into the regime $\lambda_j = \mathcal{O}(\varepsilon)$ where secondary and tertiary bifurcations occur.

Using this extended reduction, we showed that the transcritical bifurcation is typically followed by a supercritical Hopf bifurcation of the emerging pattern, similarly to the situation for (1.1) [7]. Additionally, we applied our approach to two systems with codimension 2 (transcritical) bifurcations, finding that the planar CMR must be extended to either a 3- or a 4-dimensional ECMR attracting small initial conditions exponentially. Motivated by simulations of (1.1) in [5], we have explored various scenarios for the presence of chaotic dynamics in the ECMR flow. Our approach enabled us to construct several such explicit examples, where the full PDE semiflow limits to a low-dimensional chaotic attractor, i.e. in which the full model exhibits low-dimensional chaotic spatio-temporal dynamics governed by ECMR flows — see Figs. 1.2 and 5.3(b).

This paper has a distinctive exploratory character. We have chosen to investigate the phenomena exhibited by singularly perturbed PDE systems pushed beyond the region of validity of classical CMR associated with a transcritical bifurcation: our analysis is entirely formal. Nevertheless, the backbone of our presentation

provides in itself a solid foundation for a rigorous validation. This validation is part of future work, at least for the codimension 1 case of Section 4 where a scalar CMR extends to a planar ECMR. In the context of reaction–diffusion equations, especially, results on the convergence of solutions to N-dimensional Galerkin projections as $N \to \infty$ seem directly applicable to the present setting, see e.g. [23,24]. For the codimension 2 case, it is natural to first work out in detail the general case, where eigenfunctions may not span the invariant subspace of the bifurcating eigenvalue. In that situation, one needs to account for generalized eigenfunctions, and we have refrained from doing so in the present paper.

Another line of future research concerns the application of ECMR to models where the primary bifurcation, associated with the first large eigenvalue λ_1 crossing the imaginary axis, is not transcritical. In principle, ECMR is directly applicable – at least formally – when the trivial state is annihilated/destabilized in a pitchfork or saddle–node bifurcation. Further, although that state cannot undergo a Hopf bifurcation by virtue of $\mathcal{L}$ having been assumed self-adjoint (see A1 in Section 2), a spatially inhomogeneous one could sustain it. We already emphasized that ECMR is enabled by the structure of the spectrum and not by particulars of the basic state. In principle, then, ECMR can also cover this case, as long as the spectrum has a large/small decomposition as depicted in Fig. 1.1. A natural question in all of these three contexts is whether the primary bifurcation is also typically followed by a destabilizing Hopf bifurcation already upon an $\mathcal{O}(\varepsilon)$ variation of the bifurcation parameter. This scenario indeed appears natural, see below; it will thus be relevant to study what ECMR can yield in those situations.

Since the present paper was inspired by the appearance of low-dimensional spatio-temporal dynamics in model (1.1), we finally consider the question of how assistive can ECMR be in understanding analytically the rich spatio-temporal dynamics of evolutionary PDE systems. Such dynamics are routinely observed in simulations of systems such as (1.3), see for instance [25] and references therein for often encountered reaction–diffusion cases. Scenarios involving a stationary pattern that bifurcates from a basic state, only to be destabilized in a Hopf bifurcation, also appear naturally in reaction–diffusion equations; see, for instance, [26] for an explicit example. A major question is, of course, how typical is the existence of a stability problem with small and large eigenvalues? A related question is whether the (assumed) existence of such a partition can be used to embed these systems into the singularly perturbed framework necessary for our approach. Given the character of ECMR, we are convinced that it can be applied to explicit (reaction–diffusion) models found in the literature — by assuming certain scaling limits, of course. The most natural candidates are those of Gierer–Meinhardt and Gray–Scott type, which already have the desired singularly perturbed nature; see, for instance, [27–29] and references therein. The complex dynamics exhibited by these systems is largely dominated by singular solutions of pulse type [30,31], the spectral stability problem of which does decompose into small and large eigenvalues (on bounded domains) — see, for instance, [32,33]. Typically, these pulses are destabilized through Hopf bifurcations; one thus needs to adapt ECMR to singular patterns, see our remark above on the nature of the basic state. This appears to be a promising line for future research, especially since the low-dimensional chaotic behavior exhibited by solitary pulses in an extended Gierer–Meinhardt model seems to be driven by large-small spectrum interactions [31].

Acknowledgment

LS thanks NWO for making this research possible by a grant through the NDNS+ cluster.

Appendix. Sub- or supercritical Hopf bifurcation

In this appendix the character of the Hopf bifurcation as derived in Section 4.1 is determined in full detail. We follow the procedure outlined in [16].

The system that we consider is the subsystem of the first two equations of (4.2) on the invariant center manifold.

$$\begin{cases} a_1' = ra_1 + C_{111}\left(F_{20}a_1^2 + F_{11}a_1b_1 + F_{02}b_1^2\right), \\ b_1' = -M_1 b_1 + \beta a_1. \end{cases} \tag{A.1}$$

The corresponding Jacobian of (A.1) is,

$$J(a_1, b_1) = \begin{pmatrix} r + 2C_{111}F_{20}a_1 + C_{111}F_{11}b_1 & C_{111}\left(F_{11}a_1 + 2F_{02}b_1\right) \\ \beta & -M_1 \end{pmatrix}. \tag{A.2}$$

The nontrivial stationary state that becomes stable after the transcritical bifurcation is given in (4.3). Evaluated at this stationary state, the Jacobian (A.2) is:

$$J(a_1^*, b_1^*) = \begin{pmatrix} \frac{r}{H}\left(H - 2F_{20} - \frac{F_{11}\beta}{M_1}\right) & -\frac{r}{H}\left(F_{11} + 2\frac{F_{02}\beta}{M_1}\right) \\ \beta & -M_1 \end{pmatrix},$$

see (3.13) for the definition of H. The eigenvalues of this Jacobian as a function of bifurcation parameter r are,

$$\Lambda_\pm = \frac{\operatorname{tr}(J(r)) \pm i\sqrt{4\det(J(r)) - \operatorname{tr}^2(J(r))}}{2} = \mu(r) \pm i\omega(r),$$

where $\operatorname{tr}(J(r))$ and $\det(J(r))$ represent the trace and the determinant of J in terms of r, respectively. We find that,

$$\operatorname{tr}(J(r)) = \frac{r\left(H - 2F_{20} - \frac{F_{11}\beta}{M_1}\right)}{H} - M_1,$$
$$\det(J(r)) = rM_1.$$

The Hopf bifurcation occurs if $\mu(r_H) = 0$ and $\omega(r_H) = \omega_0 > 0$, where r_H is the value of r at the bifurcation. The first condition is satisfied for

$$r_H = \frac{M_1 H}{-F_{20} + F_{02}\beta^2/M_1^2}.$$

The value of $\omega(r)$ at the bifurcation value is

$$\omega(r_H) = \omega_0 = \sqrt{r_H M_1}.$$

For $\gamma < -\nu_1$, the sign of M_1 is positive, so the requirement for a Hopf bifurcation is that

$$r_H > 0.$$

The following two degeneracy conditions must be satisfied to assure that the Hopf bifurcation is regular.

(C1) $l_1(r_H) \neq 0$, where l_1 is the first Lyapunov coefficient;
(C2) $\mu'(r_H) \neq 0$.

The sign of the first Lyapunov coefficient determines the character of the Hopf bifurcation. If $l_1(r_H) < 0$, the bifurcation is supercritical. That indicates that stable limit cycles bifurcate from the Hopf bifurcation. If $l_1(r_H) > 0$, the bifurcation is subcritical.

Condition (C2) is satisfied for all values of F_{ij} and β, because

$$\mu'(r_H) = \frac{-F_{20} + \frac{F_{02}\beta^2}{M_1^2}}{2H} = \frac{M_1}{r_H}.$$

And if $r_H > 0$, the value $\mu'(r_H)$ is always positive.

Computing the first Lyapunov coefficient is a more involved task. First we translate the variables such that the Hopf bifurcation occurs at the origin. We introduce

$$x_1 = a_1 - a_1^*, \quad \text{and} \quad x_2 = b_1 - b_1^*,$$

with a_1^* and b_1^* the values of the nontrivial stationary state, evaluated at the Hopf bifurcation, i.e. with $r = r_H$. System (A.1) then transforms into

$$\begin{cases} x_1' = r_H x_1 + C_{111}\left[F_{20}\left(x_1^2 + 2a_1^* x_1\right) \right. \\ \qquad \left. + F_{11}\left(x_1 x_2 + a_1^* x_2 + b_1^* x_1\right) + F_{02}\left(x_2^2 + 2b_1^* x_2\right)\right] \\ \quad \equiv F_1(x_1, x_2), \\ x_2' = -M_1 x_2 + \beta x_1 \equiv F_2(x_1, x_2). \end{cases} \tag{A.3}$$

Define the symmetric multilinear vector functions of $u, v, w \in \mathbb{R}^2$,

$$B(u, v) = \begin{pmatrix} B_1(u, v) \\ B_2(u, v) \end{pmatrix},$$

$$C(u, v, w) = \begin{pmatrix} C_1(u, v, w) \\ C_2(u, v, w), \end{pmatrix}$$

with

$$B_i(u, v) = \sum_{j,k=1}^{2} \frac{\partial^2 F_i((x_1, x_2)^T, r_H)}{\partial x_j \partial x_k}\bigg|_{\substack{u_j v_k \\ x_1 = x_2 = 0}},$$

and

$$C_i(u, v, w) = \sum_{j,k,l=1}^{2} \frac{\partial^3 F_i((x_1, x_2)^T, r_H)}{\partial x_j \partial x_k \partial x_l}\bigg|_{\substack{u_j v_k w_l \\ x_1 = x_2 = 0}}.$$

For (A.3), these multilinear forms are

$$B(u, v) = \begin{pmatrix} C_{111}\left(F_{20} u_1 v_1 + F_{11} u_1 v_2 + F_{11} u_2 v_1 + 2F_{02} u_2 v_2\right) \\ 0 \end{pmatrix},$$

$$C(u, v, w) = \begin{pmatrix} 0 \\ 0 \end{pmatrix}.$$

Then the system (A.3) can be represented as

$$x' = J(r_H)x + \frac{1}{2}B(x, x) + \frac{1}{6}C(x, x, x).$$

Define the eigenvectors of $J(r, H)$ and $J^T(r_H)$, q and p respectively, as

$$J(r_H)q = i\omega_0 q, \qquad J^T(r_H)p = -i\omega_0 p.$$

A straightforward computation yields that,

$$q = \begin{pmatrix} M_1 + i\omega_0 \\ \beta \end{pmatrix},$$

and with normalization $\langle p, q\rangle = 1$,

$$p = \frac{1}{2\beta M_1}\begin{pmatrix} \beta \\ M_1 + i\omega_0 \end{pmatrix}.$$

Three inner products of these eigenvectors with the multilinear forms are

$$g_{20} = \langle p, B(q, q)\rangle,$$
$$g_{11} = \langle p, B(q, \bar{q})\rangle,$$
$$g_{21} = \langle p, C(q, q, \bar{q})\rangle.$$

The first Lyapunov coefficient is defined as,

$$l_1(r_H) = \frac{1}{2\omega_0^2}\Re\left(ig_{20}g_{11} + \omega_0 g_{21}\right). \tag{A.4}$$

Computing all inner products and evaluating l_1, we find

$$l_1(r_H) = \frac{C_{111}^2}{2\omega_0 M_1^2}\left[\left(2M_1F_{20} + F_{11}\beta\right)\left(HM_1^2 + \omega_0^2 F_{20}\right)\right].$$

The factor $\frac{C_{111}^2}{2\omega_0 M_1^2}$ is positive because ω_0 is positive, so the sign of the first Lyapunov coefficient is determined by the sign of

$$\left(2M_1F_{20} + F_{11}\beta\right)\left(HM_1^2 + \omega_0^2 F_{20}\right).$$

This means that the Hopf bifurcation occurring at $r = r_H$ is

supercritical if $\left(2M_1F_{20} + F_{11}\beta\right)\left(HM_1^2 + \omega_0^2 F_{20}\right) < 0$,

subcritical if $\left(2M_1F_{20} + F_{11}\beta\right)\left(HM_1^2 + \omega_0^2 F_{20}\right) > 0$.

References

[1] P.W. Bates, C.K.R.T. Jones, Invariant manifolds for semilinear partial differential equations, in: Dynamics Reported, in: Series in Dynamical Systems, vol. 2, 1989, pp. 1–38.
[2] J. Carr, Applications of Centre Manifold Theory, in: Applied Mathematical Sciences, vol. 35, Springer–Verlag, 1981.
[3] A. Vanderbauwhede, G. Iooss, Center Manifold Theory in Infinite Dimensions, in: Dynamics Reported, vol. 1, Springer–Verlag, 1992.
[4] G.J.M. Pieters, H.M. Schuttelaars, On the nonlinear dynamics of a saline boundary layer formed by throughflow near the surface of a porous medium, Physica D 237 (2008) 3075–3088.
[5] J. Huisman, N.N. Pham Thi, D.M. Karl, B.P. Sommeijer, Reduced mixing generates oscillations and chaos in the oceanic deep chlorophyll maximum, Nature 439 (2006) 322–325.
[6] A. Zagaris, A. Doelman, N.N. Pham Thi, B.P. Sommeijer, Blooming in a non-local, coupled phytoplankton-nutrient model, SIAM J. Appl. Math. 69 (2009) 1174–1204.
[7] A. Zagaris, A. Doelman, Emergence of steady and oscillatory localized structures in a phytoplankton-nutrient model, Nonlinearity 24 (2011) 3437–3486.
[8] A. Doelman, L. Sewalt, A. Zagaris, The effect of slow spatial processes on emerging spatiotemporal patterns, Chaos (2015) in press.
[9] F. Gazzola, H.C. Grunau, G. Sweers, Polyharmonic Boundary Value Problems, in: Lecture Notes in Mathematics, vol. 1991, Springer–Verlag, 2010.
[10] E.N. Lorenz, Deterministic, non-periodic flow, J. Atmos. Sci. 20 (1963) 130–141.
[11] C. Sparrow, The Lorenz Equations: Bifurcations, Chaos and Strange Attractors, in: Applied Mathematical Sciences, vol. 41, Springer–Verlag, 1982.
[12] J.D. Gibbon, M.J. McGuinness, The real and complex Lorenz equations in rotating fluids and lasers, Physica D 5 (1982) 108–122.
[13] D. Gilbarg, N.S. Trudinger, Elliptic Partial Differential Equations of Second Order, in: Grundlehren der mathematischen Wissenschaften, vol. 224, Springer–Verlag, 1983.
[14] W. Eckhaus, Asymptotic Analysis of Singular Perturbations, in: Studies in Mathematics and its Applications, vol. 9, North-Holland, 1979.
[15] J.K. Kevorkian, J.D. Cole, Multiple Scale and Singular Perturbation Methods, in: Applied Mathematical Sciences, vol. 154, Springer–Verlag, 1996.
[16] Yu. A. Kuznetsov, Elements of Applied Bifurcation Theory, third ed., in: Applied Mathematical Sciences, vol. 112, Springer–Verlag, 2004.
[17] A. Dhooge, W. Govaerts, Yu.A. Kuznetsov, H.G.E. Meijer, B. Sautois, New features of the software matcont for bifurcation analysis of dynamical systems, Math. Comput. Model. Dyn. Syst. 14 (2) (2008) 147–175.
[18] S.N. Chow, J.K. Hale, Methods of Bifurcation Theory, in: Grundlehren der Mathemtischen Wissenschaften, vol. 251, Springer–Verlag, 1982.
[19] N. Fenichel, Geometric singular perturbation theory for ordinary differential equations, J. Differential Equations 31 (1979) 53–98.
[20] C.K.R.T. Jones, Dynamical Systems, in: Lecture Notes in Mathematics, vol. 1609, Springer–Verlag, 1995, pp. 44–118 (Chapter Geometric Singular Perturbation Theory).
[21] T.J. Kaper, An introduction to geometric methods and dynamical systems theory for singular perturbed problems, in: J. Cronin, R.E. O'Malley (Eds.), Analyzing Multiscale Phenomena Using Singular Perturbation Methods, in: Proc. Symposia of Applied Mathematics, vol. 56, American Mathematical Society, 1999, pp. 85–132.
[22] J. Guckenheimer, P. Holmes, Nonlinear Oscillations, Dynamical Systems and Bifurcations of Vector Fields, in: Applied Mathematical Sciences, vol. 42, Springer–Verlag, 1983.
[23] J.C. Robinson, Infinite–Dimensional Dynamical Systems, in: Cambridge Texts in Applied Mathematics, 2001.
[24] R. Temam, Infinite-Dimensional Dynamical Systems in Mechanics and Physics, in: Applied Mathematical Sciences, vol. 68, Springer–Verlag, 1988.
[25] R. Kapral, K. Showalter, Chemical Waves and Patterns, Kluwer, 1995.
[26] S.I. Ei, H. Izuhara, M. Mimura, Infinite dimensional relaxation oscillation in aggregation-growth systems, Discrete Contin. Dyn. Syst. Ser. B 17 (2012) 1859–1887.
[27] W. Chen, M.J. Ward, Oscillatory instabilities of multi-spike patterns for the one-dimensional Gray–Scott model, Eur. J. Appl. Math. 20 (2009) 187–214.

[28] T. Kolokolnikov, J. Wei, M. Winter, Existence and stability analysis of spiky solutions for the Gierer–Meinhardt system with large reaction rates, Physica D 238 (2009) 1695–1710.
[29] A. Doelman, F. Veerman, An explicit theory for pulses in two component, singularly perturbed, reaction–diffusion equations, J. Dynam. Differential Equations (2013) 1–41.
[30] Y. Nishiura, D. Ueyama, Spatio-temporal chaos for the Gray–Scott model, Physica D 150 (2001) 137–162.
[31] F. Veerman, A. Doelman, Pulses in a Gierer–Meinhardt equation with a slow nonlinearity, SIAM J. Appl. Dyn. Syst. 12 (2013) 28–60.
[32] D. Iron, M.J. Ward, J. Wei, The stability of spike solutions to the one-dimensional Gierer–Meinhardt model, Physica D 150 (2001) 25–62.
[33] H. van der Ploeg, A. Doelman, Stability of spatially periodic pulse patterns in a class of singularly perturbed reaction–diffusion equations, Indiana Univ. Math. J. 54 (2005) 1219–1301.